

# Implementation and Validation of Inertial Measurement Units in marker-based and marker-less 3D motion tracking

Bachelor-thesis  
by

Marius Henkel

July 19, 2016, Munich

Supervising tutor Simi: Dipl.-Kfm. Philipp Russ

Supervising tutor FH: Dr.-Ing. Steinhauser  
Second supervising tutor FH: Dr. Lehner



Department of  
Applied Sciences and  
Mechatronics



# Selbstständigkeitserklärung

Hiermit erkläre ich, Marius Henkel, geboren am 15.03.1991 in München, gemäß der Rahmenprüfungsordnung der Hochschule München, dass ich die vorliegende Arbeit mit dem Titel "Implementation and Validation of Inertial Measurement Units in marker-based and marker-less 3D motion tracking" selbstständig verfasst, noch nicht anderweitig für Prüfungszwecke vorgelegt, keine anderen als die angegebenen Quellen oder Hilfsmittel benutzt, sowie wörtliche und sinngemäße Zitate als solche gekennzeichnet habe.

Ort, Datum

Unterschrift

## Sperrvermerk

Die vorliegende Bachelorarbeit enthält vertrauliche Daten und Informationen der Simi Reality Motion GmbH, die nicht für die Öffentlichkeit bestimmt sind. Der Inhalt der Arbeit, auch auszugsweise, darf nur mit Genehmigung der Simi Reality Motion Systems GmbH an Dritte außerhalb der Hochschule München weitergegeben werden.

## Abstract

Analyzing human movements via camera based 3D-tracking has reached a turning point recently. The conventional method of motion tracking is based on retro-reflective markers, that are placed on the applicants body to highlight important points. It is being relieved by a newer approach with a camera based marker-less silhouette tracking to analyze movements easier and quicker. One major problem of this silhouette method is the tracking of rotations in body-parts, where the silhouette hardly changes, e.g. the upper and lower arm or the upper and lower legs. The solution discussed in this thesis is based on inertial measurement units, that are able to measure rotations when placed on body-parts. Furthermore the sensors are analyzed in their behavior towards the magnetic field and problems such as an offset in z-direction are discussed. After the integration of sensor-data in 3D-tracking programs (Simi Motion and Simi Shape) the data was processed and used to support silhouette tracking. Therefore sensors were placed on pelvis, thorax, upper arm right, lower arm right and wrist right and their rotations recorded. Sensor-data was compared to marker data from the same movements by the means of a correlations coefficient calculated with Spearman's rule. To validate the sensors data and the consistency of the outcome, a golf swing and a tennis forehand/backhand was recorded with the same set-up during two different days of capture. Markers were placed based on the same model on the applicants body and the movements were recorded with an eight camera system. Both marker data and IM-sensor data was then compared to each other. In a second step, marker- and IM-sensor-data was used to support rotations in the tracking process of the silhouette method. Those hybrid-trackings no longer consist of data from solely one method, but two methods mixed with each other. Results of the study show, that the integration of IM-sensors into silhouette tracking can work as good as marker-based tracking if the sensors behave well. On the other hand the sensors do not behave in the same way during both captures, meaning that only recordings of day one were correlating strongly to marker data. IM-sensor data of day two did not correlate in a strong way but only weak or no correlations were calculated at all. A possible reason to this problem was found to be the inconsistent magnetic field which is affected by electrical devices and ferric surroundings. Although nothing changed visually during both captures, only one capture resulted in good data. Concluding the thesis, IM-sensors can be integrated and used in 3D-tracking programs and support silhouette tracking in a hybrid way as good as markers, if the sensors work well. That is, the use of the sensors has to be viewed critically, especially if consistent accurate data is needed.

# Contents

|  |           |
|--|-----------|
| <b>List of Figures</b>   | <b>8</b>  |
| <b>List of Tables</b>  | <b>10</b> |
| <b>I. Introduction and Motivation</b>                                    | <b>13</b> |
| <b>1. Introduction into the fields of movement applications</b>          | <b>13</b> |
| 1.1. Evaluation of marker-less tracking . . . . .                        | 13        |
| 1.2. Evaluation of IMU-based tracking . . . . .                          | 13        |
| 1.3. Motivation and aim of thesis . . . . .                              | 14        |
| 1.3.1. Motivation for an implementation of IMUs in Simi Motion . . . . . | 14        |
| 1.3.2. Motivation for an implementation of IMUs in Simi Shape . . . . .  | 15        |
| <b>II. Implementing IMUs into Simi Motion</b>                            | <b>16</b> |
| <b>2. Theoretical approach</b>   | <b>16</b> |
| 2.1. Simi Motion marker-based tracking . . . . .                         | 16        |
| 2.1.1. marker placement . . . . .  | 17        |
| 2.2. IMU-based tracking . . . . .  | 18        |
| 2.2.1. Rotations . . . . .   | 19        |
| 2.3. Combining IM-sensors with 'Motion' . . . . .                        | 19        |
| 2.3.1. Coordinate Transformation . . . . .                               | 20        |
| 2.3.2. Zero positioning . . . . .  | 20        |
| 2.4. Basic anatomy . . . . .   | 21        |
| 2.4.1. Anatomical axes and planes . . . . .                              | 21        |
| 2.4.2. Human joints and their movement possibilities . . . . .           | 22        |
| 2.5. IM-sensor based problems and their solutions . . . . .              | 24        |
| 2.5.1. Z-offset: background information . . . . .                        | 24        |
| 2.5.2. Z-offset: possible causes . . . . .                               | 25        |
| 2.5.3. Z-offset: solution . . . . .                                      | 26        |
| 2.5.4. Sensor-calibration: background information . . . . .              | 29        |
| 2.5.5. Magnetic field . . . . .  | 31        |

|   |           |
|---|-----------|
| <b>3. Materials</b>   | <b>32</b> |
| 3.1. Software . . . . .   | 32        |
| 3.2. Hardware . . . . .   | 32        |
| <b>4. Methods</b>   | <b>33</b> |
| 4.1. Setup and Calibration . . . . .                              | 33        |
| 4.2. Marker- and IM-sensor-placement . . . . .                    | 33        |
| 4.3. IM-sensor: Pre-movement initialization . . . . .             | 34        |
| 4.4. Recorded Movements and Data comparison . . . . .             | 35        |
| 4.5. Spearman’s correlation coefficient . . . . .                 | 35        |
| 4.6. Data processing . . . . .                                    | 37        |
| <b>5. Results</b>   | <b>38</b> |
| 5.1. Golf swing capture day one . . . . .                         | 39        |
| 5.1.1. Comparison of Marker and IMUs: Pelvis . . . . .            | 39        |
| 5.1.2. Comparison of Marker and IMUs: Thorax . . . . .            | 39        |
| 5.1.3. Comparison of Marker and IMUs: Upper arm right . . . . .   | 40        |
| 5.1.4. Comparison of Marker and IMUs: Lower arm right . . . . .   | 41        |
| 5.1.5. Comparison of Marker and IMUs: Wrist right . . . . .       | 41        |
| 5.1.6. Comparison of Shape and IMUs: Pelvis . . . . .             | 41        |
| 5.1.7. Comparison of Shape and IMUs: Thorax . . . . .             | 42        |
| 5.1.8. Comparison for Shape and IMUs: Upper arm right . . . . .   | 43        |
| 5.1.9. Comparison of Shape and IMUS: Lower arm right . . . . .    | 43        |
| 5.1.10. Comparison of Shape and IMUs: Wrist . . . . .             | 43        |
| 5.2. Tennis forehand capture day one . . . . .                    | 44        |
| 5.2.1. Pelvis: IMUs and markers, IMUs and Shape . . . . .         | 44        |
| 5.2.2. Thorax: IMUs and markers, IMUs and Shape . . . . .         | 44        |
| 5.2.3. Upper arm: IMUs and markers, IMUs and Shape . . . . .      | 45        |
| 5.2.4. Lower arm: IMUs and markers, IMUs and Shape . . . . .      | 45        |
| 5.2.5. Wrist: IMUs and markers, IMUs and Shape . . . . .          | 46        |
| 5.3. Golf swing capture day two . . . . .                         | 46        |
| 5.3.1. Pelvis: IMUs and marker, IMUs and Shape . . . . .          | 47        |
| 5.3.2. Thorax: IMUs and marker, IMUs and Shape . . . . .          | 47        |
| 5.3.3. Upper arm right: IMUs and marker, IMUs and Shape . . . . . | 48        |
| 5.3.4. Lower arm right: IMUs and marker, IMUs and Shape . . . . . | 48        |
| 5.3.5. Wrist right: IMUs and marker, IMUs and Shape . . . . .     | 49        |

|             |   |           |
|-------------|---|-----------|
| 5.4.        | Tennis backhand capture day two . . . . .                           | 49        |
| 5.4.1.      | Pelvis: IMUs and marker, IMUs and Shape . . . . .                   | 49        |
| 5.4.2.      | Thorax: IMUs and marker, IMUs and Shape . . . . .                   | 50        |
| 5.4.3.      | Upper arm right: IMUs and marker, IMUs and Shape . . . . .          | 50        |
| 5.4.4.      | Lower arm right: IMUs and marker, IMUs and Shape . . . . .          | 51        |
| 5.4.5.      | Wrist right: IMUs and marker, IMUs and Shape . . . . .              | 51        |
| <b>6.</b>   | <b>Discussion</b>   | <b>51</b> |
| 6.1.        | Total correlations of capture day one and two . . . . .             | 52        |
| <b>III.</b> | <b>Implementing IMUs into Simi Shape</b>                            | <b>56</b> |
| <b>7.</b>   | <b>Extended Theory</b>  | <b>56</b> |
| 7.1.        | Silhouette tracking in Simi Shape . . . . .                         | 56        |
| 7.1.1.      | Implementing IMUs into marker-less tracking Simi Shape . . . . .    | 57        |
| <b>8.</b>   | <b>Additional Methods</b>   | <b>59</b> |
| 8.1.        | marker-less tracking . . . . .                                      | 59        |
| 8.2.        | hybrid marker-based tracking . . . . .                              | 60        |
| 8.3.        | hybrid IMU-based tracking . . . . .                                 | 62        |
| <b>9.</b>   | <b>Results</b>  | <b>64</b> |
| 9.1.        | Golf swing capture day one . . . . .                                | 64        |
| 9.1.1.      | Pelvis: Hybrid marker-Shape and hybrid IMU-Shape . . . . .          | 64        |
| 9.1.2.      | Thorax: Hybrid marker-Shape and hybrid IMU-Shape . . . . .          | 65        |
| 9.1.3.      | Upper arm right: Hybrid marker-Shape and hybrid IMU-Shape . . . . . | 65        |
| 9.1.4.      | Lower arm right: Hybrid marker-Shape and hybrid IMU-Shape . . . . . | 66        |
| 9.1.5.      | Wrist right: Hybrid marker-Shape and hybrid IMU-Shape . . . . .     | 66        |
| 9.2.        | Tennis forehand capture day one . . . . .                           | 66        |
| 9.2.1.      | Pelvis: Hybrid marker-Shape and hybrid IMU-Shape . . . . .          | 66        |
| 9.2.2.      | Thorax: Hybrid marker-Shape and hybrid IMU-Shape . . . . .          | 67        |
| 9.2.3.      | Upper arm right: Hybrid marker-Shape and hybrid IMU-Shape . . . . . | 67        |
| 9.2.4.      | Lower arm right: Hybrid marker-Shape and hybrid IMU-Shape . . . . . | 67        |
| 9.2.5.      | Wrist right: Hybrid marker-Shape and hybrid IMU-Shape . . . . .     | 68        |

|   |           |
|---|-----------|
| 9.3. Golf and Tennis capture day two . . . . .  | 68        |
| 9.3.1. Pelvis: Hybrid marker-Shape and marker for golf and tennis backhand . . . . .          | 68        |
| 9.3.2. Thorax: Hybrid marker-Shape and marker for golf and tennis backhand . . . . .          | 69        |
| 9.3.3. Upper arm right: Hybrid marker-Shape and marker for golf and tennis backhand . . . . . | 69        |
| 9.3.4. Lower arm right: Hybrid marker-Shape and marker for golf and tennis backhand . . . . . | 69        |
| 9.3.5. Wrist right: Hybrid marker-Shape and marker for golf and tennis backhand . . . . .     | 70        |
| <b>10. Discussion</b>   | <b>70</b> |
| 10.1. Comparison of hybrid marker-shape data of capture day two . . . . .                     | 72        |
| <br>  |           |
| <b>IV. Conclusion</b>   | <b>74</b> |

## List of Figures

|     |   |    |
|-----|---|----|
| 1.  | high end matrixvision camera with a mounted ringlight . . . . .   | 16 |
| 2.  | Tools for calibration: Wand and L-frame [1, p.104] . . . . .  | 17 |
| 3.  | Marker positions in the inverse kinematics model . . . . .  | 18 |
| 4.  | Three planes of the body [2] . . . . .  | 21 |
| 5.  | Examples of the six synovial joints in the human body [3] . . . . .   | 23 |
| 6.  | possible joint movements [4] . . . . .  | 23 |
| 7.  | Different Offsets in z-direction: IMUs (black) point towards different north-poles while compass (grey) shows actual north-pole . . . . . | 24 |
| 8.  | Z-offset of six IM-sensors at the 20-seconds-mark . . . . .   | 25 |
| 9.  | Z-offset compared to x- and y-offset of 2 sensors . . . . .   | 27 |
| 10. | 10 calibrations of sensor 2 compared 10 offset-acquisitions . . . . .   | 30 |
| 11. | Z-offset of six IM-sensors in an in-door tennis facility . . . . .  | 31 |
| 12. | Example of Spearmans calculation in Libre Office calc, Pelvis IMU and Marker data is compared . . . . .                                   | 36 |
| 13. | Pelvis movement filtered with 6Hz vs 10 Hz . . . . .  | 38 |
| 14. | X-, Y- and Z-values of the pelvis based on IMU-data . . . . .   | 39 |
| 15. | IM-sensor Z-values of pelvis and thorax are presented . . . . .   | 40 |
| 16. | Z-rotations of Shape-data compared to IM- and marker-based data . . . . .   | 42 |
| 17. | Table with correlation coefficients of total values for golf swing day one . . . . .  | 52 |
| 18. | Comparison of lower arms during IMU-initialization: actual position (right) vs. IM-based model (left) . . . . .                           | 53 |
| 19. | Total correlation coefficients from the tennis forehand on capture day one . . . . .  | 53 |
| 20. | Total correlation coefficients from the golf swing on capture day two . . . . .   | 54 |
| 21. | Total correlation coefficients compared from the golf swing on capture days one and two . . . . .   | 54 |
| 22. | Total correlation coefficients compared from the tennis movements on capture days one and two . . . . .                                   | 55 |
| 23. | tilted hip during tennis forehand movement . . . . .  | 58 |
| 24. | tilted arm during golf pre-swing phase movement . . . . .   | 59 |
| 25. | Initialized markers on Shape-model for hybrid marker-based silhouette tracking . . . . .  | 62 |
| 26. | IM-sensor settings in 'Shape' X=red, Y=green, Z=blue . . . . .  | 63 |



|     |   |    |
|-----|---|----|
| 27. | Total correlation coefficients from hybrid-marker and -imu data during golf swing on day one . . . . .                | 71 |
| 28. | Total correlation coefficients from hybrid-marker and -imu data during tennis forehand on day one . . . . .           | 71 |
| 29. | Total correlation coefficients from hybrid-marker and -imu data during golf and tennis forehand on day one . . . . .  | 72 |
| 30. | Total correlation coefficients from hybrid-marker data during golf swing day one and two . . . . .                    | 73 |
| 31. | Total correlation coefficients from hybrid-marker data during tennis forehand / backhand on day one and two . . . . . | 73 |

## List of Tables

|     |   |    |
|-----|---|----|
| 1.  | IM-sensor Calibration . . . . .   | 30 |
| 2.  | Cohen's Spearman classification . . . . .   | 37 |
| 3.  | Adapted Spearman classification . . . . .   | 37 |
| 4.  | Spearman correlation of IM-sensors and Marker data: Pelvis . . . . .                        | 39 |
| 5.  | Spearman correlation of IM-sensors and Marker data: Thorax . . . . .                        | 40 |
| 6.  | Spearman correlation of IM-sensors and Marker data: Upper arm right .                       | 40 |
| 7.  | Spearman correlation of IM-sensors and Marker data: Lower arm right .                       | 41 |
| 8.  | Spearman correlation of IM-sensors and Marker data: Wrist right . . . .                     | 41 |
| 9.  | Spearman correlation of IM-sensors and silhouette data: Pelvis . . . . .                    | 42 |
| 10. | Spearman correlation of IM-sensors and silhouette data: Thorax . . . . .                    | 42 |
| 11. | Spearman correlation of IM-sensors and silhouette data: Upper arm right                     | 43 |
| 12. | Spearman correlation of IM-sensors and silhouette data: Lower arm right                     | 43 |
| 13. | Spearman correlation of IM-sensors and silhouette data: Wrist . . . . .                     | 44 |
| 14. | Spearman correlation of IM-sensors and marker/silhouette data: Pelvis .                     | 44 |
| 15. | Spearman correlation of IM-sensors and marker/silhouette data: Thorax                       | 45 |
| 16. | Spearman correlation of IM-sensors and marker/silhouette data: Upper<br>arm right . . . . . | 45 |
| 17. | Spearman correlation of IM-sensors and marker/silhouette data: Lower<br>arm right . . . . . | 46 |
| 18. | Spearman correlation of IM-sensors and marker/silhouette data: Wrist<br>right . . . . .     | 46 |
| 19. | Spearman correlation of IM-sensors and marker/silhouette data: Pelvis .                     | 47 |
| 20. | Spearman correlation of IM-sensors and marker/silhouette data: Thorax                       | 47 |
| 21. | Spearman correlation of IM-sensors and marker/silhouette data: Upper<br>arm right . . . . . | 48 |
| 22. | Spearman correlation of IM-sensors and marker/silhouette data: Lower<br>arm right . . . . . | 48 |
| 23. | Spearman correlation of IM-sensors and marker/silhouette data: Wrist<br>right . . . . .     | 49 |
| 24. | Spearman correlation of IM-sensors and marker/silhouette data: Pelvis .                     | 49 |
| 25. | Spearman correlation of IM-sensors and marker/silhouette data: Thorax                       | 50 |
| 26. | Spearman correlation of IM-sensors and marker/silhouette data: Upper<br>arm right . . . . . | 50 |

|     |  |    |
|-----|--|----|
| 27. | Spearman correlation of IM-sensors and marker/silhouette data: Lower arm right . . . . . | 51 |
| 28. | Spearman correlation of IM-sensors and marker/silhouette data: Wrist right . . . . .     | 51 |
| 29. | Spearman correlation of hybrid silhouette data: Pelvis . . . . .                         | 64 |
| 30. | Spearman correlation of hybrid silhouette data: Thorax . . . . .                         | 65 |
| 31. | Spearman correlation of hybrid silhouette data: Upper arm right . . . . .                | 65 |
| 32. | Spearman correlation of hybrid silhouette data: Lower arm right . . . . .                | 66 |
| 33. | Spearman correlation of hybrid silhouette data: Wrist right . . . . .                    | 66 |
| 34. | Spearman correlation of hybrid silhouette data: Pelvis . . . . .                         | 66 |
| 35. | Spearman correlation of hybrid silhouette data: Thorax . . . . .                         | 67 |
| 36. | Spearman correlation of hybrid silhouette data: Upper arm right . . . . .                | 67 |
| 37. | Spearman correlation of hybrid silhouette data: Lower arm right . . . . .                | 67 |
| 38. | Spearman correlation of hybrid silhouette data: Wrist right . . . . .                    | 68 |
| 39. | Spearman correlation of hybrid silhouette data: Pelvis . . . . .                         | 68 |
| 40. | Spearman correlation of hybrid silhouette data: Thorax . . . . .                         | 69 |
| 41. | Spearman correlation of hybrid silhouette data: Upper arm right . . . . .                | 69 |
| 42. | Spearman correlation of hybrid silhouette data: Lower arm right . . . . .                | 69 |
| 43. | Spearman correlation of hybrid silhouette data: Wrist right . . . . .                    | 70 |

## List of abbreviations

| Abbreviation | Meaning                               |
|--------------|---------------------------------------|
| 2D/3D        | 2/3-Dimensional                       |
| approx.      | Approximately                         |
| C7           | Cervical spine 7                      |
| COG          | Center of gravity                     |
| COM          | Center of motion                      |
| csv          | Comma separated values                |
| EMG          | Electromyography                      |
| ENU          | East-North-Up                         |
| etc.         | Et cetera                             |
| IM           | Inertial measurement                  |
| IMUs         | Inertial measurement units            |
| INS          | Inertial Navigation Systems           |
| ISB          | International Society of Biomechanics |
| L            | Left                                  |
| LED          | Light emitting diode                  |
| pry          | Pitch roll yaw                        |
| R            | Right                                 |
| ROM          | Range of motion                       |
| $r_s$        | Spearman's correlation coefficient    |
| SO(3)        | Special orthogonal group              |
| V2           | Aggregate-4 / Vergeltungswaffe 2      |

# Part I.

## Introduction and Motivation

### 1. Introduction into the fields of movement applications

This section will give a brief overview of background information concerning this thesis.

#### 1.1. Evaluation of marker-less tracking

Technology in motion capture seems to have reached a turning point in recent years, merging from marker-based applications in various fields to marker-less applications. One significant example is Microsoft's kinect system, to replace the outdated controller with a camera based motion capture device. It helps selecting options in the menu through gesture detection or is used in-game. Apart from changes in the gaming industry, motion capture and furthermore movement analysis is also shifting in many clinical applications and sports medicine. However a recent study shows, that a single-camera system like the kinect is not suitable for a motion analysis that relies on high quality data and high accuracy.[5] Like the marker-based version, marker-less applications commonly use a four to eight camera system. In the case of Simi's 'Shape', a silhouette-subtracting algorithm calculates position and movement of body parts during a movement analysis [6, p.21] Other than marker-based systems, 'Shape' is not in need of any marker or sensor placement and thus does not need any extra time for marker placement nor is it prone to any placement errors. A latterly study on the comparison between marker-based and marker-less movements shows, that angle differences above a Range of Motion [ROM] of  $5^\circ$  in all joints show correlations between 70 and 100 percent. This excludes ankle eversion/inversion and abduction/adduction as well as shoulder rotation and elbow flexion/extension, where the angles hardly correlate.[7]

#### 1.2. Evaluation of IMU-based tracking

Especially in astro-navigation and avigation, inertial measurement units [IMUs] have a long history to look upon. A rudimentary version was already used in the second World War, where it could estimate position and heading of V2-rockets.[8] The system

## 1. Introduction into the fields of movement applications

was later on used not only in military- or astro-systems but also in aviation and naval navigation. One well-known example is the Delco carousel, that was installed in the inertial navigation systems [INS] of the early Boeing 747-100, -200 and -300 versions.[9] Those IMU-systems used gimbals, which contained expensive precision parts and a set of three rings, attached to each other in an  $90^\circ$ -angle. This construction with the sensor placed in the middle of the inner ring, makes a rotation around any axis possible. Alongside the high costs, this setup had a restriction called gimbal lock. Here, two rings are aligned to each other, making a rotation around the third axis coincide with another axis. A solution to this problem is a 'strapped-down' system, in which the sensor is connected directly to the vehicle. This system not only eliminates the problem with the gimbal lock, but is also much more cost efficient and can be used in much smaller sizes. Like marker-less tracking, IMUs are starting to become more and more recognized in clinical-applications and especially sports medicine. These matchbox-sized sensors are easily attachable to body-parts or any piece of sports equipment and can measure position, accelerations and rotations.

### 1.3. Motivation and aim of thesis

Aim of this thesis is to analyze and integrate IMU sensors in an already existing motion capture and analysis software. The sensors are then validated via two different sets of movements in the two programs 'Motion' and 'Shape' to see, if their collected data is better, equal or worse than the data collected with 'Motion' and 'Shape'. For a better lucidity, this thesis will be separated into three major parts. Part I will cover everything that is connected to the IMU-implementation into Simi Motion. Part II will then use the progress and knowledge of part I to focus solely on the implementation of the IMUs in Simi Shape. Part III will summarize parts I and II and conclude the thesis. For this thesis the IMU-sensors from Delsys were used.

#### 1.3.1. Motivation for an implementation of IMUs in Simi Motion

Although the integration and hybrid-use of sensors in 'Shape' seems more interesting, an implementation of the sensors in 'Motion' is of vital use. Not only does the software already have an data-acquisition tool, that is synced to the camera capture, but also does 'Shape' use the room-calibration, recorded and executed in 'Motion'. Any data, that is used in 'Shape', will first be recorded and sometimes even edited in 'Motion'. Therefore an implementation of the IMUs in 'Shape' does not work without first implementing

## *1. Introduction into the fields of movement applications*

them in 'Motion'. In addition to that 'Motion' offers another advantage: it has the tools to calculate inverse kinematics solely from the IMUs, without any marker-placement or camera-recording. Summing up, 'Motion' is not only needed for 'Shape', but can also record either markers and sensors hybrid, or also solely markers or sensors.

### **1.3.2. Motivation for an implementation of IMUs in Simi Shape**

As introduced in section 1.1, marker-less tracking is becoming a game-changer in future motion analysis. The ability to also use the system outdoors with less needed time for preparation makes 'Shape' an important feature in all current fields of application. One problem that 'Shape' still faces is to record rotations of shoulder and elbow, as well as inversion/eversion of the ankle. That is due to the fact, that during those movements, the actual shape of these body-parts hardly changes. A possible solution to this problem could be IMU-sensors, as are they able to record position and rotations of the segments, they are attached to. This additional part of information could help 'Shape' to interpret certain movements or stabilize the tracking of other body-parts like the feet or the hip. This hybrid tracking version is still in no need of any additional markers and can also be used in outdoor-settings.

## Part II.

# Implementing IMUs into Simi Motion

## 2. Theoretical approach

This chapter will focus on the theoretical aspects of the thesis. It will cover all the background-information of the different systems used and describes the theory behind the methods.

### 2.1. Simi Motion marker-based tracking

Simi's software 'Motion' is a multi-functional tool to capture different sets of data and process them for further use either in other programs such as 'Shape', or to output the data in reports. The most important feature is the camera-based capture with up to eight cameras in conventional setups. Special setups might require more cameras, which is only a matter of hardware and thus not mentioned any further. The cameras have ring-lights mounted on top of them, casting light-emitting diode [LED]-light in the direction, the camera is pointing at.



Figure 1: high end matrixvision camera with a mounted ringlight

The subject to be recorded is wearing retro-reflecting, spherical markers, that are attached via adhesive tape to certain points of his body. The LED-light coming from



## 2. Theoretical approach

the cameras is reflected by the markers and captured by the cameras. The cameras have to be set up in such a way, that during every movement, every marker can be seen from at least two cameras. [10, p.31] Otherwise the computer can not calculate the 3D position of the marker. The System is calibrated with a L-shaped frame with four markers attached, as well as a wand with three markers attached. The markers on the L-frame give information about the global coordinate system, used during marker-based and marker-less capturing. The long leg of the 'L' points in y-direction, the short leg in x-direction. This information will then be calculated in the computer to create the z-axis perpendicular to both legs pointing in the air. The information of the wand is used to distort the cameras in the area of movement. Therefore the distance between the three markers will tell the computer, which distances there are in the area of movement.



Figure 2: Tools for calibration: Wand and L-frame [1, p.104]

### 2.1.1. marker placement

Markers are used to calculate estimate forces and torques in each segment of the human body with the method of inverse dynamics. Therefore the human body is divided up into 16 segments, which are: foot(Left [L]/Right [R]), shank(L/R), thigh(L/R), wrist(L/R), lower arm(L/R), upper arm(L/R) as well as head, upper and lower torso and pelvis. All segments are connected with joints. With a predefined marker-set, marker positions and orientations can be determined with the video-images captured. The inner forces and torques can then be calculated from this information. [1, p.347] [11] The markers also inform, where each joint is positioned, as well as the center of gravity [COG] of each segment. Those centers are used as the origin of the segment's local coordinate system.

## 2. Theoretical approach

The joint-centers of ankle, knee, elbow and wrist are located right in the middle of each joint's medial and lateral marker. Joint-centers of hip and shoulders are calculated with a different, more complex method described by Bell, et al. [12] and De Leva [13]. Like the segments, joints have local coordinates, too. They are based on standards from the International Society of Biomechanics [ISB]. In this study a full body, inverse kinematics marker-set was used.

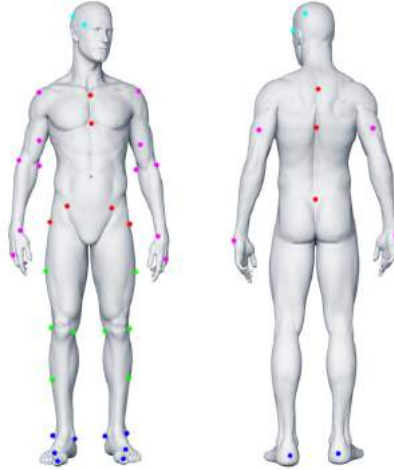


Figure 3: Marker positions in the inverse kinematics model

### 2.2. IMU-based tracking

As mentioned previously, IMUs from Delsys were used in this thesis. The Inertial measurement [IM]-feature of these sensors is a recent add-on to the already existing Electromyography [EMG]-function. As those sensors have been integrated into Simi's Motion software a longer time ago, the change to an integration of the additional IM-feature was less work, than to integrate a whole new sensor. Like mentioned in section 1.2., the sensors are a strapped-down version of their older gimbal-precursor. The IM-sensors record three different data types from three different sensors, that can be converted into different forms of rotation-matrices, such as quaternions or the pitch-roll-yaw [pry] data. The three different sensors within the IM-sensor are: one gyroscope, one accelerometer and one magnetometer. Each sensor collects data in x-, y- and z-direction, which equals a total of nine data-channels.

The gyroscope measures rotation angles around its internal x-, y- and z-axis. The accelerometer collects accelerations of the sensor but cannot collect gravitational accelerations. The magnetometer collects information about the magnetic field, the sensors

## 2. Theoretical approach

is used in. [14, p.3]

### 2.2.1. Rotations

For this set-up quaternions were recorded, which contain four channels of information. They are divided in one real path which has information about the orientation, as well as three imaginary paths, that give information about the rotations around x-, y- and z-axis. These four dimensional rotations are used, because they have one extra set of information about the orientation, compared to the special orthogonal group [SO(3)], which is used in Simi Motion or any other three dimensional rotations such as euler angles. This circumvents the problem of gimbal-locks, where two rotation-axis fall together.

For example, if a plane would pitch  $90^\circ$ , its roll-axis(x) and the gravitational-axis (yaw = z) fall together.

If in this setup, the plane rotates around its roll-axis, both yaw and roll look alike and can therefore not be separated anymore.[15, p.114-118] [16, p.3]

IM-sensors have two different sets of coordinate systems, in which they express rotations: an internal one, that has its y-axis pointing in the direction of the arrow on the sensor, its x-axis pointing perpendicular to y to the right, leaving the z-axis pointing perpendicular to x and y in the air. The second coordinate system is used as a reference system and is, other than the internal coordinate system, stationary. This system is the East-North-Up [ENU]-coordinate system, with x pointing towards the global East, y pointing towards the global north-pole and z pointing perpendicular to x and y in the air. [17] Rotations are then calculated as rotations around the internal axis in relation to the ENU-system.

Simi Motion works with rotations in the SO3-format of the Lie-algebra, so a standard transformation from quaternions into SO(3)-format is performed automatically, when the sensor-rotations are imported. [1, p.245]

## 2.3. Combining IM-sensors with 'Motion'

Aided by the previous section on the basic knowledge of how Motion and IM-sensors work, this section will focus on the theoretical aspects connected to the combination of IM-sensor data acquisition and the software component 'Motion'.

## 2. Theoretical approach

### 2.3.1. Coordinate Transformation

As described in section 2.2.1., IM-sensors use two different coordinate systems to express rotations. Rotations are recorded as rotations around the IMUs internal coordinate system in reference to the global ENU-coordinate system.

Rotations (in this case segment rotations) in Motion are also described as rotations around an internal coordinate system compared to a global coordinate system. The difference is, that segment- or joint-rotations are calculated with markers in the inverse dynamics calculation as rotations around the segment/joint coordinate system compared to the global coordinate system in Motion. This global coordinate system is defined by the L-frame during calibration and can vary from setup to setup depending on movement direction and therefore L-frame-placement. So not only the sensor compared to the segments/joints has a different internal coordinate system, but also the reference coordinate systems differ. So if sensors are placed on the human body alongside markers for a recording, two different sets of rotations are recorded, although the subject only performs one move.

In order to get the same set of rotations, the systems have to be transformed, so that in the end both methods use the same internal and global coordinate system. There are two solutions to this problem: using the ENU-coordinate system as the common global system or using 'Motion's' coordinate system defined by the L-frame during calibration. This means either the L-frame has to be set for every calibration to point to the north or the IM-sensors have to be geared to the L-frame.

For practical reasons, that will be presented in section 3.4., solution two is used in this thesis. That is the L-frame will be used as the global coordinate system.

### 2.3.2. Zero positioning

Once the global systems are aligned, both markers and IM-sensors use the same reference but still have different internal coordinate systems. Measurements show, that IM-sensors have their point of origin, when lying flat on the ground, all axis being aligned with their global coordinate system. The internal coordinate system of all segments and joints have their point of origin, when the subject stands in the anatomical neutral position, facing in the y-direction of the L-frame.

So just by placing the IM-sensors on their assigned segments will not record the same rotations. The internal coordinate systems have to be transformed like the global coordinate systems. In this thesis the IM-coordinate system is transformed into the

## 2. Theoretical approach

joint-coordinate system. From this point on this procedure is referred to as "zeroing" or "zero-positioning"

### 2.4. Basic anatomy

#### 2.4.1. Anatomical axes and planes

The anatomy uses three major body-axes to describe orientation and position of any segments. All axes meet in an idealized Center of motion [COM]. They are:

- Longitudinal-axis: y-axis of the body, going from cranial to caudal or the other way around.
- Sagittal-axis: z-axis of the body, going through the body from back to front.
- Transversal-axis: x-axis of the body, going from either the COM towards the left or right half of the body or from the left body half of the body to the right half of the body.

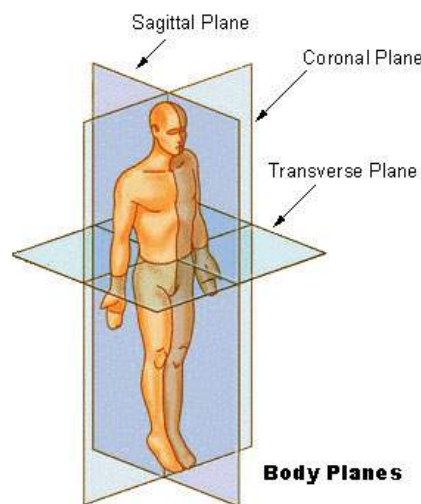


Figure 4: Three planes of the body [2]

Two axes span one plane, which leads to the three body planes:

- Frontal-plane/Coronal-plane: longitudinal- and transversal-axis form this plane
- Sagittal-plane: both sagittal- and longitudinal-axis form this plan which divides the body into two symmetrical halves

## 2. Theoretical approach

- Transversal-plane: transversal- and sagittal-axis span this plane, which divides the body in upper and lower body.

### 2.4.2. Human joints and their movement possibilities

In the human body, bones are connected to each other through joints. Muscles are attached to the bones through tendons and enable movements. Joints can be divided into two major groups, the real joints, also called diarthrosis or synovial-joints and false joints, also called synarthrosis. Only real joints have a joint space and three characteristic features.

- Joint cavity: synovial fluid inside the joint space
- Joint capsule: a fibrous capsule around the joint, that protects the joint and prevents the fluid from pouring out.
- hyaline cartilage: cartilage around the bone ends that form the joint

There are six major joint types which can be divided into three classes depending on their degrees of freedom. Ball joints are the only joints that can move anywhere, as they have three degrees of freedom. Condyloid joints as well as plane joints and saddle joints form the second group with only two possible degrees of freedom. In the third group there are hinge- and pivot-joints, which only have one degree of freedom. Figure 5 shows all six joints with possible examples in the human joint system.

## 2. Theoretical approach

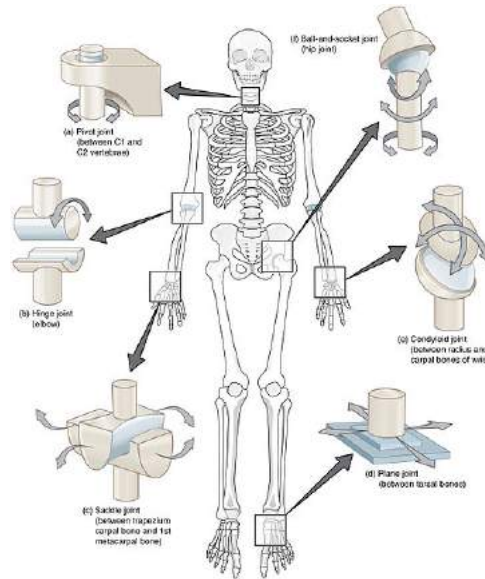


Figure 5: Examples of the six synovial joints in the human body [3]

Joint-movements are called differently according to which axis they rotate around. Movements around the sagittal-axis in the frontal-/coronal-plane are called ab-/adduction, movements around the transversal-axis in the sagittal-plane are called flexion/extension and finally rotations around the longitudinal-axis in the transversal-plane are called inversion/eversion. Figure 6 shows all possible movements.

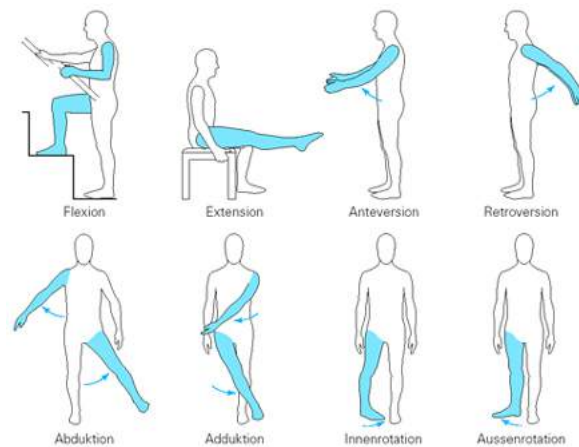


Figure 6: possible joint movements [4]

## 2.5. IM-sensor based problems and their solutions

As mentioned in sections 2.3.1. and 2.3.2. the IM-sensors use different coordinate systems than 'Motion' and thus have to be transformed. This procedure is not only a mathematical problem but also a practical one, because 'Motion' only offers a solution to one problem.

In addition to that, the IM-sensors manifest various issues, that have to be solved in advance, to ensure correct data acquisition.

### 2.5.1. Z-offset: background information

One of the biggest issues, the IM-sensors have, is an inexplicable offset in z-direction. It was mentioned earlier, that each sensor has its point of origin, when being aligned with the ENU-coordinate system. That is, they are lying flat on the floor, pointing with the arrow towards the north-pole. The problem now is, that every sensor seems to detect a different north-pole, meaning all arrows point in a different direction. Figure 7 shows this problem, as all sensors point in a different direction. A compass was used to detect the actual north-pole.



Figure 7: Different Offsets in z-direction: IMUs (black) point towards different north-poles while compass (grey) shows actual north-pole

The sensor-layout shown in Figure 7 can be achieved by laying the sensors flat on the floor, all next to each other, pointing in the same direction. If then data acquisition is started in Motion, a live-view shows the z-offset of every single sensor. The sensors can then be turned around their z-axis, until the z-value is approximately 0 rad.



## 2. Theoretical approach

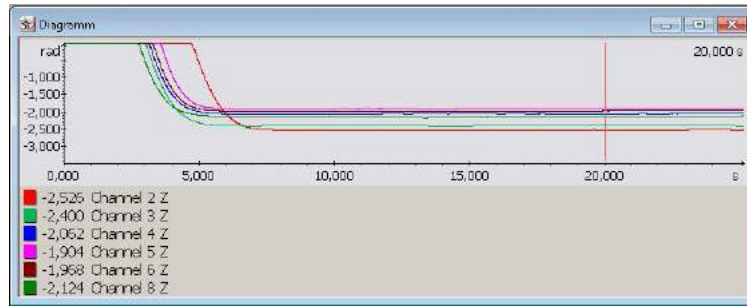


Figure 8: Z-offset of six IM-sensors at the 20-seconds-mark

Another good visualization for this problem is the data itself, as it can be seen after recording in Motion. Figure 8 shows such an offset in rad/s with six IM-sensors used.

The moment of 20 s was chosen, because various measurements show, that the sensors take time to initialize. This usually is the case after 10 s, but another 10 s were added as a precaution. Sensor 1 (red) has the smallest offset with -2.526 rad, Sensor 4 (pink) has the biggest with -1.904 rad. So the difference between biggest and smallest offset is 0,627 rad which equals approx.  $35,638^\circ$ .

### 2.5.2. Z-offset: possible causes

Like mentioned before, this problem seems to be inexplicable, especially because the offsets vary from time to time. Nevertheless there are some influences, that help create this problem.

- Magnetic field: like the compass, the sensors orientate themselves through their three magnetometers at the magnetic field. The field can be influenced by various things, such as electricity or ferrous objects. The laboratory, that was used during data acquisition, contains not only ferrous objects like a desk, but also a computer, cameras and their electrical wires, force plates and a treadmill. Those items change the magnetic field in an unpredictable way.
- Sensor calibration: like mentioned in the next section, the each sensor is calibrated before its use. Every sensor has to be calibrated manually that is, two calibrations will never be the same. In addition to that, the calibration tool does not really give a clue, if the calibration was performed well or not.
- Constructional errors: all sensors look alike, only their assigned numbers differ. This does not include the inside of the sensors, which can not be looked at. As

## 2. Theoretical approach

the sensors are highly susceptible to all kinds of influences, tiny errors during production could make them change their behavior.

### 2.5.3. Z-offset: solution

Although the issue seems to inexplicable, there is a solution to this problem. The offset can be measured after every calculation and does not change as long as the sensors stay in the same spot and are not re-calibrated.

Before every data acquisition, the offset of the sensors has to be measured and can then be used to perform a coordinate transformation of the actual movement. This will not only solve the offset-issue, but also be part of the global coordinate transformation. This transformation can be achieved in two different ways, each having advantages and disadvantages.

#### Mathematical transformation

The mathematical correct version calculates with normal an inverse matrices. The actual movement data will be called  $M$ , the new one  $M^T$  while the z-offset is  $O$  or  $O^{-1}$  for inverse z-offset.

$$M^T = O^{-1} * M * O \quad (1)$$

When calculating with matrices, it is important in which order they are multiplied with each other, because the commutative law does not apply. So the offset-matrix is first inverted and calculated onto the movement-matrix from the left ( $M$  is the center-matrix). After this step, the original offset-matrix has to be multiplied with  $M$  from the right to get the transformed matrix  $M^T$ . The advantages of this way are:

- Mathematical correctness. Every moment in time is used to calculate a new set of data at this exact moment. Therefore no error is produced.
- Calculation tools, which are offered already in Motion and do not need to be calculated in a different program like Excel.

Although this way is mathematically correct, there is one major disadvantage, too:

- The calculation-tool in 'Motion' only calculates data from two data-rows for the time-span, that both rows overlap. This means, either both data rows have to have the exact same length, or the offset-measurement has to be longer, than the actual movement-acquisition. If the offset-data-row is shorter in time than the

## 2. Theoretical approach

movement-acquisition, the extra time will still include the offset. Although the offset-data can be stretched in time by reducing the frame rate, the user always has to know exactly how long he acquired data. Also alongside the stretching, there are multiple steps needed, to transform the offset data with the movement data including inverting the offset and calculating for every single sensor by itself. A request for a more user friendly use was started .

- Another smaller disadvantage is the time, as the sensors do not only have to initialize during the offset measurement, but also during movement-acquisition. For the movement-acquisition, an initialization time of 20 seconds is used, to ensure, that the sensors initialized right. This extra time has to be taken into consideration when measuring the offset in this way.

Summing up, the method uses precise calculations with tools from 'Motion' to give precise transformed data, but is very limited in terms of extra time or second/third, etc. tries.

### Turning system of coordinates

The second way is a more practical approach, using an important fact of the offset-problem. Measurements show, that the offset only appears in z-direction, x- and y-coordinates are zero.

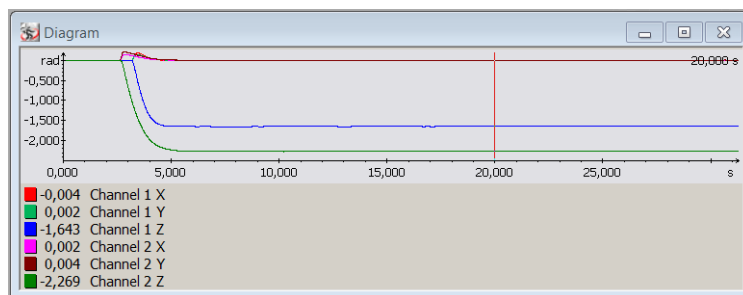


Figure 9: Z-offset compared to x- and y-offset of 2 sensors

Figure 9 shows, that during the offset-measurement, sensor 1 has an offset of  $-0,004$  rad (or  $-0,229^\circ$ ) in x-direction (red) and  $0,002$  rad (or  $0,115^\circ$ ) in y-direction (green). These small differences are more like a noise, than a significant value like the z-offset. Sensor 2 is approximately [approx.] the same. This means, that the coordinate system is just turned around the z-axis, but the x-y-plane remains the same. For the second way, 'Motion' offers a tool, that turns the coordinate system around one specific axis.

## 2. Theoretical approach

Again the method only works in this case, because solely one axis is affected. In a way this method does the same thing as way number one, just in a more practical approach. The advantages are:

- One value (mean-value of the offset) from each sensor is needed to perform this step and it only takes one step to perform this calculation.
- The procedure is time-independent, therefore it can be added to the calibration as a standardized procedure for any movement-acquisition.

Like the other method, this way also inherits disadvantages:

- This method needs one value in ( $^{\circ}$ ), around which the coordinate system is turned. For this value, the mean-value from the time-span 10 s to 30 s is used and recalculated from radiant into degrees. Also the standard deviation is calculated to see, if the sensors are drifting and have to be re-calibrated. This is usually the case when the standard deviation is above  $1,5^{\circ}$ . Normal standard deviations vary from  $0,20$  to  $1,0^{\circ}$ . 'Motion' does not yet offer tools to calculate mean-value or standard deviation simply by executing one calculation. The calculation-template, that is needed for this action, is not yet written so the calculations for this step are performed in Excel (or in case of this thesis with Libre Office Calc).

To get the z-offsets from 'Motion' into 'Calc', they are exported as a .txt file.

- The method inherits a mathematical error, as only the mean-value is used. The standard deviation shows, which error this is.
- The calculation needs one extra step in a program like Excel and can not yet be performed solely in 'Motion'.

Although the second methods inherits a mathematical error, this error is usually so small, that it can be neglected. The advantage to use this method as a standardized procedure in addition to calibration for any movements outbalances the disadvantages and is thus used in this thesis. With the outlook on an upcoming calculation template, this method will also be faster than method one. Both methods share one advantage and one disadvantage: both methods eliminate the z-offset problem and are at the same time used for the global-coordinate-transformation. The disadvantage is, that every step has to be performed for each sensor separately, therefore more sensors take longer to correct, than fewer ones.

This method does not necessarily require a camera recording, as long as all sensor face in the exact same direction during the offset measurement.

#### 2.5.4. **Sensor-calibration: background information**

Another inexplicable issue is the sensor calibration. It is performed before data-acquisition in an external software called 'Delsys IM Sensor Calibration' and then loaded into the software 'Trigno Control Utility'. In the Magnetometer calibration, the user traces a sphere in the place of movement by performing eight-shaped movements. After this step is repeated for every sensor, the sensors are then placed on the floor to perform the Accelerometer calibration. All sensors are recorded together in this step. After calibration, the file is exported in a comma separated file [.csv]-file. There are several problems:

- Calibration is performed manually, therefore no sensor will be calibrated in the same way like the others.
- The newest calibration-software tells the user in a percentage from 0 to 100 percent, how good or bad a calibration was performed. However, all sensors roughly get the same percentage every time, no matter how good or bad they were actually calibrated.
- The calibration-file can be manipulated in a way, that every sensor has the exact same calibration-data. This does not affect the z-offset of this calibration, though.
- The quality of the calibration can not be linked to the z-offset, but if the z-offset has one outlier, this problem can usually be solved by re-calibrating the sensors.

To show, that all sensors get roughly the same calibration each time, a test with six IM-sensors was performed. All six sensors were calibrated 10 times and the quality noted. After 10 calibrations, the mean value and standard deviation were calculated.

## 2. Theoretical approach

Table 1: IM-sensor Calibration

| Calibrations    | Channel 1 | Channel 2 | Channel 3 | Channel 4 | Channel 5 | Channel 6 |
|-----------------|-----------|-----------|-----------|-----------|-----------|-----------|
| 1               | 90,76     | 87,07     | 91,92     | 89,05     | 95,33     | 82,54     |
| 2               | 91,21     | 86,70     | 91,29     | 86,80     | 91,24     | 85,87     |
| 3               | 92,77     | 87,78     | 92,21     | 86,77     | 93,28     | 85,25     |
| 4               | 91,92     | 88,13     | 92,52     | 90,23     | 92,95     | 84,16     |
| 5               | 88,48     | 87,73     | 91,11     | 87,06     | 91,63     | 84,71     |
| 6               | 90,62     | 88,78     | 93,09     | 84,63     | 94,58     | 89,30     |
| 7               | 90,54     | 88,40     | 90,74     | 88,33     | 91,67     | 86,17     |
| 8               | 91,58     | 89,15     | 92,52     | 89,25     | 93,10     | 87,24     |
| 9               | 90,90     | 88,89     | 90,93     | 88,59     | 93,50     | 84,50     |
| 10              | 91,70     | 88,09     | 90,93     | 88,59     | 93,50     | 84,50     |
| Mean value in % | 91,05     | 88,07     | 91,75     | 87,92     | 93,01     | 85,18     |
| S.dev. in %     | 1,13      | 0,78      | 0,81      | 1,61      | 1,29      | 2,15      |

*calibrations performed with eight sensors in %*

Table 1 shows, that no matter how often the sensors are re-calibrated, the standard deviation is only 2.15 % at the max.

Between every calibration, the z-offset was measured, to see if the quality can be linked to the offset. When comparing Channel 2 with its calibrations, no pattern can be spotted.

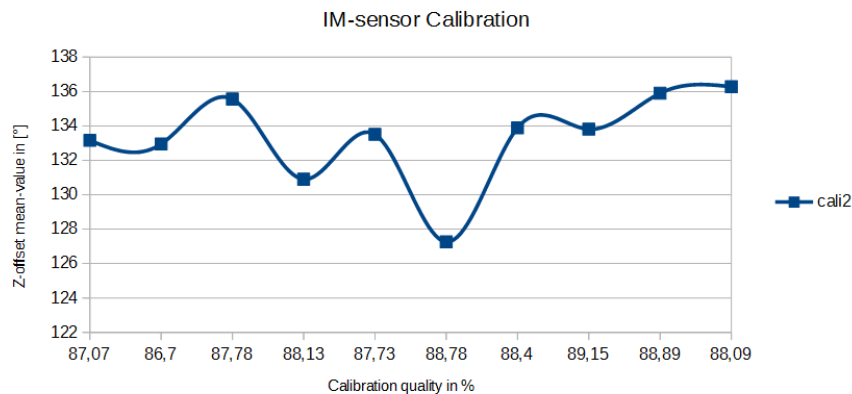


Figure 10: 10 calibrations of sensor 2 compared 10 offset-acquisitions

### Sensor-calibration: solution

Although the calibration is a faulty procedure, that does not give any hints, if the sensors are calibrated well or bad, it does not create any further problems either. It

## 2. Theoretical approach

is not possible, to link the bad calibration-procedure to the offset problem solely with acquisitions and 'Motion'. Therefore it will not be mentioned in this thesis any further.

### 2.5.5. Magnetic field

In section 2.5.2., the magnetic field was already mentioned to cause possible problems concerning the z-offset. This section will cover some findings about the magnetic field. As mentioned previously, the sensors use their built-in magnetometers to orientate in the magnetic field of the earth. Although the magnetic field is defined by north- and south-pole, it is not homogeneous, as it can be diverted by different causes. These causes include ferromagnetic diversions such as ferric parts of a table, supports in a house's wall or the roof. In addition electric devices like cellphones, computers or any parts and wires connected to them change the magnetic field temporarily. Especially small rooms or gait-analysis laboratories with many cameras, force-plates, a treadmill and complimentary computers can not secure a nearly homogeneous magnetic field. Section 2.5.1 hints, that these changes might affect the z-offset.

A measurement in an in-door tennis court supports this theory.



Figure 11: Z-offset of six IM-sensors in an in-door tennis facility

Figure 11 shows, that at the time-mark of 20 s, the offset of the sensors to each other is only 0,137 rad equaling approx.  $7,87^\circ$ . Compared to the offset mentioned above with almost  $36^\circ$ , the difference is notably big. In this case of measurement, all cameras and the computer were placed at least 7 meters and 20 meters at the max from the movement area. This proves, that in wider areas of movement with cameras and computers further away, the IM-sensors do have a smaller offset to each other.

Summing up, this section shows, that in larger areas of movement or even outdoors, the sensors will get notable better results. The recordings from this thesis were acquired in a small lab with close-up cameras, force-plates and computers, though.

## 3. Materials

This section will give an overview of software and hardware used in this thesis. Part one and two use the same materials, therefore they will only be mentioned once.

### 3.1. Software

- Simi Motion 9.2.1 RC1 for calibration, marker- and IMU-tracking
- Simi Shape 2.2.1 RC4 for silhouette-tracking
- Libre Office Calc for calculating and averaging the IM-offset as well as calculating the Spearman-correlation
- Delsys Trigno Control Utility version 2.5
- Delsys Calibration for Sensor calibration (comes with Trigno Control Utility)

### 3.2. Hardware

- Simi Motion Calibration tools: L-frame and T-Wand
- 44x 12,5 mm reflective markers for inverse kinematics
- 8x Basler scA 640-120cg cameras with up to 120 Hz of frame rate and a resolution of 658x492 pixels
- 8x ringlights with 72 LEDs each
- 8x Fujinon 3.8-13 mm DV3.4x3.8SA-1 lenses
- 1x IO-Box for camera and ringlights power-supply and integrated National Instruments trigger-board
- each one power-cable and one Ethernet-cable per camera
- 5-8 Delsys IM-sensors depending on the recordings
- one Delsys Trigno-Station for IM-sensor recording connected via USB to the computer
- one Computer with all Software installed



## 4. Methods

Section 4. will focus on the various methods, used in this thesis. This includes the explanation of the data acquisitions as well as the statistics to compare the results.

### 4.1. Setup and Calibration

In both parts of this thesis, the same setup and calibration is used. Eight cameras were used for recording in the same setup for the two recordings. Four cameras are placed with tri-pods and clams on the floor or the wall in hip-height, two each sagittal and frontal or dorsal respectively. The additional four cameras were placed in the room corners, filming from above. This setup guarantees, that every marker and body segment can be seen at any time of recording in at least two cameras. Also all cameras are either close to the capturing area or zoomed in to have as little surroundings captured as possible. This is important, because this way arms or legs can be differentiated better.

All recordings feature the same type of calibration to distort the cameras and set the coordinate system. In this process, a wand dance is performed and processed as described in the 'Motion Manual' [10, p.30-40].

The IM-sensors were calibrated using Delsys' Calibration tool and then placed alongside the L-frame, facing all in the same direction to record their z-offset. The offset was later on calculated onto the acquired IM-movement data as described in section 2.5.3..

### 4.2. Marker- and IM-sensor-placement

Both parts use the same marker and IM-sensor-placement. 44 markers are used in this thesis for the inverse kinematics model shown in figure 3 in section 2.1.1.. Except for the two toe-markers, which are only needed for the static model initialization, all other 42 markers were used during every acquisition.

During all acquisitions, five IM-sensors were used to record rotations in different segments. In every movement, the sensors were placed on the same segments:

- Pelvis: Sensor one was placed on the mid spina iliaca posterior, underneath the lower back marker. This sensor will record pelvic rotations and support especially marker-less tracking at this position. Also the two movements recorded rely on quality hip information.
- Thorax / Cervical Spine 7 [C7]: Sensor two is placed underneath the C7-marker on the upper back right between the two shoulders. This sensor will record rota-

## 4. Methods

tions of the trunk and is interesting to be compared to the hip-sensor. Again the information is important for the two movements recorded. Sensors one and two both point with their arrows cranial.

- Upper arm right: Sensors three to five are placed on the right arm to gather rotational information, especially inversion and eversion of the three arm segments. Therefore all sensors are aligned alongside an axis pointing from the shoulder towards the middle finger base joint. Sensor three is placed in the middle of the upper arm between shoulder-joint marker and epicondylus lateralis marker as well as in-between biceps and triceps markers.
- Lower arm right: Sensor four is placed three-fourths of the lower arm towards the wrist joint in the middle between markers wrist lateral and medial right, being aligned with sensor five on the back of the hand. This particular placement is used to capture rotations caused by ulnar and radius in the lower arm and thus to differ from the shoulder rotations in the upper arm.
- Wrist right: Sensor five is placed on the middle finger base joint close to sensor four with the difference, that sensor five also captures rotations of the wrist-joint. Sensor five is placed on the back of the hand to prevent disturbance in the palm when holding a racket. All arm sensors have their arrows pointing towards the middle finger base joint.

The orientation of the sensors is not important for calculations but gives consistency in placement and eases some steps when used in 'Shape'.

### 4.3. IM-sensor: Pre-movement initialization

It was mentioned previously, that the IM-sensors need time to initialize themselves, before they can be used for data acquisition. Every sensor takes a different period of time to initialize and engage onto their certain offset. Usually all sensors are initialized after 10 seconds but an additional 10 seconds are used to secure that the sensors are all set. During these 20 seconds, the recorded subject needs to stand still in the neutral zero position, facing in the direction of movement. During this time, cameras and sensors are recording already.

After 20 seconds, the sensors offsets caused by their placement on the segments towards the global coordinate system are zeroed by clicking the command 'Zero positioning' in

## 4. Methods

'Motion'. The sensors X-, Y- and Z-data is then set to 0 rad and the sensors are ready to use.

### 4.4. Recorded Movements and Data comparison

In this thesis, two different movements in two different recordings were used to validate the sensors implementation and recorded data: a golf-swing as well as a tennis forehand and backhand. Recording one consists of one golf-swing and one tennis forehand, recording two of one golf-swing and a tennis backhand. Both recordings use the exact same camera setup, marker positioning and IM-sensors but were recorded on different dates.

In each recording, the following sets of data were acquired:

- IM-sensor segment rotations of pelvis, thorax, upper and lower arm right as well as wrist right
- Marker-data of the inverse kinematics model, only segment rotations of the segments mentioned above are used.
- Shape silhouette-tracking data, again only segment rotations are used
- Hybrid Shape and marker segment rotations
- Hybrid Shape and IMU segment rotations

Every segment-rotation is outputted in X-, Y- and Z-rotations which are compared to each other via a correlation coefficient. Alongside the single coordinate rotations, a total correlation of all three rotations combined is compared as well. The total correlation is also used in the second recording to decide whether a hybrid silhouette-IMU based tracking makes sense or not.

### 4.5. Spearman's correlation coefficient

For the means of data comparison, a special statistic method has to be used in this thesis. One of the most common correlations coefficient formulas was introduced by Pearson in 1865. This statistic method compares two sets of data when they are normally distributed with the help of a coefficient, that tells the user a percentage how close the data rows correlate. The data sets in this thesis are not normally distributed, though. Therefore Pearson's method does not apply. Instead a comparison by Spearman has to

#### 4. Methods

be calculated. Spearman's method is a special case of the Pearson formula, that uses ranks of the data rows instead of the data rows solely. Other than that, the same formula is applied. It reads as following:

$$r_s = \frac{\frac{1}{n} * \sum_i (rgx_i * rgy_i) - (mvr gx_i * mvr gy_i)}{sdr gx_i * sdr gy_i} \quad (2)$$

$R_s$  means Spearman's coefficient or is simply just referred to as  $\rho$  (rho). Rgx and rgy are the ranks of the data rows of X and Y which is not to be confused with the the coordinates X, Y and Z. Rgx and rgy can be the X (coordinate) data-rows of Pelvis IMU and Marker data, for example. Mvrgx is the mean value of rgx, while sdrgx the standard deviation. N is the number of samples compared [18, p.309].

Values vary from -1 to +1 with a value close to -1 being a perfect negative correlation, +1 being a perfect positive one. Coefficients close to 0 mean bad or no correlation. Like mentioned before, X, Y and Z-coordinates are used for comparison as well as a total of X,Y and Z. The total value, which describes the correlation of two segments, can not be taken as a mean value of correlation X,Y and Z but has to be calculated separately, again with the help of Spearman's formula. In this case, values of X, Y and Z are written underneath each other for each method and then compared to the other method. Figure 12 shows an example of how the coefficient is being calculated in Libre Office calc.

| W                    | X   |               | Y           |               | Z           | AA            | AB             | AC             | AD             | AE                |
|----------------------|---|---------------|-------------|---------------|-------------|---------------|----------------|----------------|----------------|-------------------|
|                      | Rank IMU X                                | Rank Marker X | Rank IMU Y  | Rank Marker Y | Rank IMU Z  | Rank Marker Y | Rank IMU Z     | Rank Marker Z  | Rank IMU total | Rank Marker total |
| Mean values          | 135,2643052                               | 134,258855586 | 110,8419619 | 145,967302452 | 115,7029973 | 106,517711172 | 394,4768392371 | 453,920809264  |                |                   |
| Standard dev.        | 118,8124223                               | 119,442013376 | 59,20393655 | 85,2960707945 | 62,75358668 | 74,5162841131 | 262,0677543541 | 313,2046994384 |                |                   |
|                      | X   | Y             | Z           | total         |             |               |                |                |                |                   |
| Spearman correlation | =(1/367 * SUMME(R5:R371) - X3*Y3)/(X5*Y5) |               |             |               |             |               |                |                |                |                   |

Figure 12: Example of Spearmans calculation in Libre Office calc, Pelvis IMU and Marker data is compared

In order to value the correlations coefficients, a classification has to be used. In the year 1980, Cohen made such a classification:

Table 2: Cohen’s Spearman classification

| $r_s$ | Interpretation      |
|-------|---------------------|
| 0,1   | weak correlation    |
| 0,3   | average correlation |
| 0,5   | strong correlation  |

*correlations coefficients with different interpretations*

This classification is not suitable for this question, as it is anticipated to have strong correlations with high values. This is due to the fact, that different tracking methods record the same movement. In order to classify data in this thesis, the module has been adapted using various sources [19] ,[20] .

Table 3: Adapted Spearman classification

| $r_s$      | Interpretation      |
|------------|---------------------|
| $\leq 0.5$ | weak correlation    |
| 0,5-0,8    | average correlation |
| $\geq 0.8$ | strong correlation  |

*correlations coefficients with different interpretations adapted for this thesis*

This classification is more suitable for the data and therefore used.

## 4.6. Data processing

After data acquisition, the data has to be processed further to ensure, all data-files have the same settings. The inverse dynamics group from the markers is calculated through a static and a dynamic calculation. For the static 3D-coordinates, all 44 markers have to be clicked in at least two cameras and then saved as a static 3D-coordinates group to serve as a initialization pose for the 3D-dynamic calculation. The inverse dynamics then inherit the segment-rotations. The inverse kinematics groups from silhouette tracking and hybrid silhouette tracking already inherits segment rotations and is automatically calculated after tracking is finished. IM-sensor data includes already the required segment rotations data. Additionally the rotations have to be converted from [rad] to degree [°]. All other segment rotations are already in degrees.

All files were recorded from 'Motion' and 'Shape' were filtered, using a second order lowpass filter with 6 Hertz [Hz]. This frequency is orientated on Richards, who rec-

## 5. Results

ommends higher cut-off frequencies for faster movements then walking but for slower movements 6 Hz [21]. Dal. Pupo et. al. as well as Wilson et. al.[22] use 10 Hz filters for faster movements such as jumps. When correlating a Pelvis data row filtered with 10 Hz to one with 6 Hz, the correlation coefficient is at  $r_s = 0.99901$ . This means that the data does hardly differ. For reasons of consistency, the 6 Hz filter was chosen.

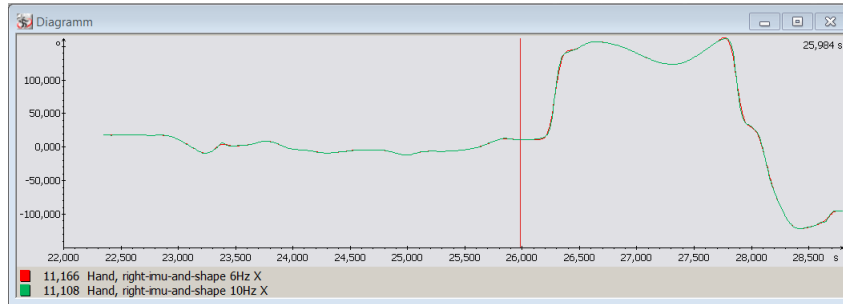


Figure 13: Pelvis movement filtered with 6Hz vs 10 Hz

One more step has to be performed before correlating data: although all methods are triggered and capture the exact same time, IM-sensors have a fixed frequency of 148.5 Hz, while all other data is captured with 100 Hz. That is IM-sensors have more samples than all other data. A time normalization is performed by resampling all data to the amount of IM-samples, because IM-sensors always record with 148.5 Hz, while data from all other methods can vary on what frequency is used for recording.

## 5. Results

In the following section, results from both capture day one and two are presented. As this part of the thesis focuses on the implementation of the IM-sensors in 'Motion', only results regarding this part are presented. Those will include pelvis, thorax, upper-, lower-arm right and wrist segment rotations of one golf hit and one tennis forehand on capture day one and a golf hit and one tennis backhand on capture day two. For each specific segment, IM-sensor data will be compared to marker data as well as to silhouette based data. The comparison will be done by means of the correlations coefficient calculated by Spearmans rule mentioned in section 4.5.

## 5.1. Golf swing capture day one

### 5.1.1. Comparison of Marker and IMUs: Pelvis

During a golf swing, pelvic rotations feature one significant rotation, which is the rotation around the Z-axis. This is because during the different swing phases, the body turns around the Z-axis in more than 180 °. Figure 14 shows, that while there is only a slight change in X and Y, the Z graph has a significant path.

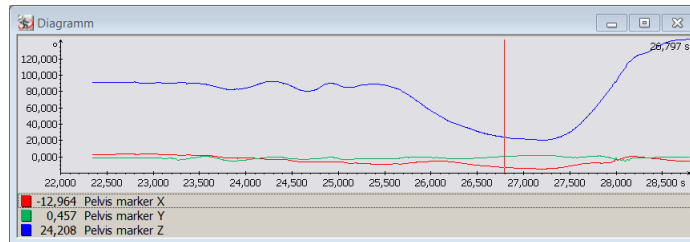


Figure 14: X-, Y- and Z-values of the pelvis based on IMU-data

Marker data of this rotations highly correlates to the IM-sensor rotations in Z-axis. Other than that, the total correlation of both methods is very close, too.

Table 4: Spearman correlation of IM-sensors and Marker data: Pelvis

| Type  | $r_s$   | Interpretation      |
|-------|---------|---------------------|
| X     | 0,90744 | strong correlation  |
| Y     | 0,72307 | average correlation |
| Z     | 0,94198 | strong correlation  |
| total | 0,96154 | strong correlation  |

*correlations coefficients of Pelvis during golf hit on capture day one*

### 5.1.2. Comparison of Marker and IMUs: Thorax

Like the pelvis, the thorax too changes most significantly in Z-direction. Rotations around Z are even stronger than in the pelvis like figure 15 shows. In this particular figure, thorax and pelvis Z-rotations of IMU data was presented. Again, a strong correlation between markers and IMUs is expected.

## 5. Results

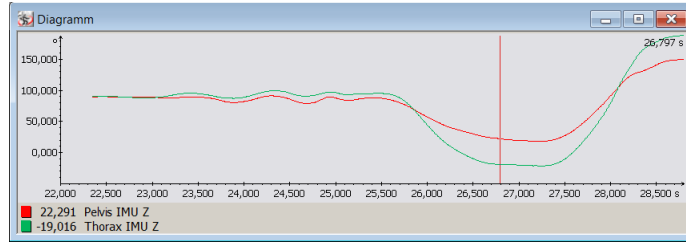


Figure 15: IM-sensor Z-values of pelvis and thorax are presented

Table 5: Spearman correlation of IM-sensors and Marker data: Thorax

| Type  | $r_s$   | Interpretation      |
|-------|---------|---------------------|
| X     | 0,88940 | strong correlation  |
| Y     | 0,58620 | average correlation |
| Z     | 0,94687 | strong correlation  |
| total | 0,95888 | strong correlation  |

*correlations coefficients of Thorax during golf hit on capture day one*

Z and total values show, that both methods also correlate strongly in this segment.

### 5.1.3. Comparison of Marker and IMUs: Upper arm right

The upper arm does not feature one significant rotation during the golf swing but all three rotations are important. For inversion and eversion rotations of a stretched out arm pointing in Y-direction, a rotation around the Y-axis has to be looked at. But as the swing does not consist of only one part where the arm is stretched out pointing forward, the inversions and eversions consist of more than one single part of rotational information.

Table 6: Spearman correlation of IM-sensors and Marker data: Upper arm right

| Type  | $r_s$   | Interpretation     |
|-------|---------|--------------------|
| X     | 0,94019 | strong correlation |
| Y     | 0,84147 | strong correlation |
| Z     | 0,93352 | strong correlation |
| total | 0,89289 | strong correlation |

*correlations coefficients of Upper arm right during golf hit on capture day one*

Again strong correlations between IM-sensor rotations and markers are present.



## 5. Results

### 5.1.4. Comparison of Marker and IMUs: Lower arm right

Although the lower arm is not integrated in the Shape part, results of the rotations will still be looked upon. Like the upper arm, the lower arm is troubling with inversions and eversions.

Table 7: Spearman correlation of IM-sensors and Marker data: Lower arm right

| Type  | $r_s$    | Interpretation            |
|-------|----------|---------------------------|
| X     | 0,56178  | average-weak correlation  |
| Y     | -0,01862 | negative weak correlation |
| Z     | 0,62024  | average correlation       |
| total | 0,79285  | average correlation       |

*correlations coefficients of Lower arm right during golf hit on capture day one*

The lower arm right is the first segment to only achieve decent correlations. Suggestions about the IMUs behavior on this particular segment will be discussed in the section 'discussion' of part one.

### 5.1.5. Comparison of Marker and IMUs: Wrist right

As the wrist features all rotations from the lower arm as well as additional flexion and extension, similar correlations like the lower arm are expected.

Table 8: Spearman correlation of IM-sensors and Marker data: Wrist right

| Type  | $r_s$   | Interpretation      |
|-------|---------|---------------------|
| X     | 0,63604 | average correlation |
| Y     | 0,51540 | average correlation |
| Z     | 0,92583 | strong correlation  |
| total | 0,88305 | strong correlation  |

*correlations coefficients of Wrist right during golf hit on capture day one*

Unlike the bad correlations of the lower arm, the wrist again has an overall strong correlation with the markers.

### 5.1.6. Comparison of Shape and IMUs: Pelvis

As especially in silhouette tracking, data of the pelvis and the arms cause trouble, their data is interesting to be looked at in terms of a comparison between 'Shape' and IM-

## 5. Results

sensor rotations. Although it is apparent that data from Shape does not correlate very good to markers, it is interesting to see, if IM-sensor data correlates to Shape data in the same way.

Table 9: Spearman correlation of IM-sensors and silhouette data: Pelvis

| Type  | $r_s$ [%] | Interpretation             |
|-------|-----------|----------------------------|
| X     | 0,32562   | weak correlation           |
| Y     | 0,54398   | average correlation        |
| Z     | 0,73456   | average correlation        |
| total | 0,825514  | average-strong correlation |

*correlations coefficients of Pelvis during golf hit on capture day one*

Figure 21 shows, that especially the significant Z-rotation is not as strong in 'Shape' as it is with markers or IM-sensors.

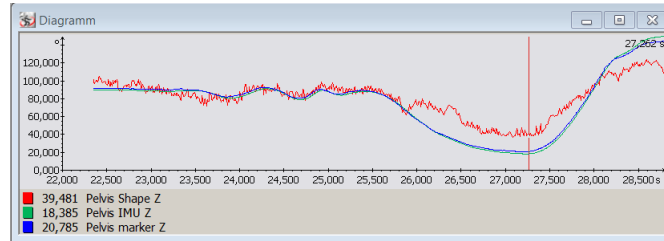


Figure 16: Z-rotations of Shape-data compared to IM- and marker-based data

### 5.1.7. Comparison of Shape and IMUs: Thorax

Other than the Pelvis, the Thorax is expected to have high correlations, because unlike the hip, the upper body is not prone to joint movements. As the shoulders are connected to the upper-body, this segment has changes in the silhouette that can be segmented better.

Table 10: Spearman correlation of IM-sensors and silhouette data: Thorax

| Type  | $r_s$ [%] | Interpretation      |
|-------|-----------|---------------------|
| X     | 0,93176   | strong correlation  |
| Y     | 0,79358   | average correlation |
| Z     | 0,89791   | strong correlation  |
| total | 0,97493   | strong correlation  |

*correlations coefficients of thorax during golf hit on capture day one*

## 5. Results

### 5.1.8. Comparison for Shape and IMUs: Upper arm right

Shape-data compared to IMU-data of the upper arm right has the following correlation coefficients:

Table 11: Spearman correlation of IM-sensors and silhouette data: Upper arm right

| Type  | $r_s$ [%] | Interpretation      |
|-------|-----------|---------------------|
| X     | 0,95295   | strong correlation  |
| Y     | 0,86620   | strong correlation  |
| Z     | 0,80321   | average correlation |
| total | 0,87774   | strong correlation  |

*correlations coefficients of upper arm right during golf hit on capture day one*

### 5.1.9. Comparison of Shape and IMUS: Lower arm right

Table 12: Spearman correlation of IM-sensors and silhouette data: Lower arm right

| Type  | $r_s$ [%] | Interpretation             |
|-------|-----------|----------------------------|
| X     | 0,061001  | average correlation        |
| Y     | 0,09891   | weak-no correlation        |
| Z     | 0,87616   | strong-average correlation |
| total | 0,54643   | average correlation        |

*correlations coefficients of Lower arm right during golf hit on capture day one*

Like the comparison of IM sensors to marker data, the comparison with the Shape-data shows average to weak correlations.

### 5.1.10. Comparison of Shape and IMUs: Wrist

During normal Shape-trackings, the wrist joint is locked to achieve more stable results. With this background information, the correlation is not expected to be good.

## 5. Results

Table 13: Spearman correlation of IM-sensors and silhouette data: Wrist

| Type  | $r_s$ [%] | Interpretation      |
|-------|-----------|---------------------|
| X     | 0,62698   | average correlation |
| Y     | 0,69091   | average correlation |
| Z     | 0,03760   | weak-no correlation |
| total | 0,29140   | weak correlation    |

*correlations coefficients of Wrist right during golf hit on capture day one*

Like expected, the correlation is weak.

### 5.2. Tennis forehand capture day one

Like the golf swing, the tennis hit was recorded with the exact same setup and right after the golf hit. Therefore the sensors behavior is not expected to change much.

#### 5.2.1. Pelvis: IMUs and markers, IMUs and Shape

Although tennis and golf are to very different sports, rotations for the pelvis are expected to show similar results to the ones from the golf swing. This is because also during a tennis hit, the body is rotated mostly around the global Z-axis. Also from this section onward, each segment will feature all comparison summed up in one section.

Table 14: Spearman correlation of IM-sensors and marker/silhouette data: Pelvis

| Method            | X              | Y              | Z       | total   |
|-------------------|----------------|----------------|---------|---------|
| IMU-marker, $r_s$ | 0,97298        | 0,83657        | 0,93685 | 0,93337 |
| Strength          | strong         | average-strong | strong  | strong  |
| IMU-Shape, $r_s$  | 0,80036        | 0,05712        | 0,93685 | 0,79750 |
| Strength          | average-strong | weak-none      | strong  | average |

*correlations coefficients of Pelvis during tennis forehand on capture day one*

Especially during the very defined Z-rotations, correlations between IMUs and markers or Shape respectively are strong.

#### 5.2.2. Thorax: IMUs and markers, IMUs and Shape

Again, during the tennis movement the upper body's movement is defined through a big rotation around the Z-axis. Therefore a look upon those data is especially interesting.

## 5. Results

Table 15: Spearman correlation of IM-sensors and marker/silhouette data: Thorax

| Method            | X       | Y       | Z       | total   |
|-------------------|---------|---------|---------|---------|
| IMU-marker, $r_s$ | 0,98822 | 0,39430 | 0,99600 | 0,95986 |
| Strength          | strong  | weak    | strong  | strong  |
| IMU-Shape, $r_s$  | 0,99294 | 0,27220 | 0,98164 | 0,95675 |
| Strength          | strong  | weak    | strong  | strong  |

*correlations coefficients of Thorax during tennis forehand on capture day one*

One significance of this data-table is, that the Y-coordinate correlation is weak in both comparisons. This shows, that if the correlation of IM-sensors to markers is weak, it will not get better when being compared to Shape-data.

### 5.2.3. Upper arm: IMUs and markers, IMUs and Shape

For the upper arm right, the following data correlations were acquired.

Table 16: Spearman correlation of IM-sensors and marker/silhouette data: Upper arm right

| Method            | X       | Y       | Z       | total   |
|-------------------|---------|---------|---------|---------|
| IMU-marker, $r_s$ | 0,97264 | 0,14588 | 0,97907 | 0,87171 |
| Strength          | strong  | weak    | strong  | strong  |
| IMU-Shape, $r_s$  | 0,98637 | 0,41392 | 0,94913 | 0,91257 |
| Strength          | strong  | weak    | strong  | strong  |

*correlations coefficients of Upper arm right during tennis forehand on capture day one*

Also in this section, both Y-data correlations are weak. This is due to IM-sensor problems.

### 5.2.4. Lower arm: IMUs and markers, IMUs and Shape

In case of the lower arm right, the following data correlations were calculated:

## 5. Results

Table 17: Spearman correlation of IM-sensors and marker/silhouette data: Lower arm right

| Method            | X       | Y            | Z         | total   |
|-------------------|---------|--------------|-----------|---------|
| IMU-marker, $r_s$ | 0,41526 | 0,42280      | 0,04978   | 0,61583 |
| Strength          | weak    | weak         | weak-none | average |
| IMU-Shape, $r_s$  | 0,39986 | 0,50276      | 0,78057   | 0,64579 |
| Strength          | weak    | average-weak | average   | average |

*correlations coefficients of Lower arm right during tennis forehand on capture day one*

Although the correlation of IMU data to Shape data is better than correlated to the marker data, the overall total correlation shows, that the data rows are by far not close to each other.

### 5.2.5. Wrist: IMUs and markers, IMUs and Shape

With the wrist being connected through a joint to the lower arm, transferring the rotations of the lower arm onto the wrist, a similar result for the wrist is expected.

Table 18: Spearman correlation of IM-sensors and marker/silhouette data: Wrist right

| Method            | X       | Y       | Z                  | total   |
|-------------------|---------|---------|--------------------|---------|
| IMU-marker, $r_s$ | 0,72214 | 0,92965 | -0,04351           | 0,72219 |
| Strength          | average | strong  | negative weak-none | average |
| IMU-Shape, $r_s$  | 0,73693 | 0,52308 | 0,33521            | 0,52087 |
| Strength          | strong  | average | weak               | average |

*correlations coefficients of Wrist right during tennis forehand on capture day one*

Although the correlations in the wrist are better than in the lower arm, both total correlations are not above average.

## 5.3. Golf swing capture day two

In this thesis, two captures on different days were performed, to see, if the data is somewhat consistent and does not change throughout the days. For this purpose, the second capture day was chosen to be two weeks after capture day one but with the exact same setup and sensors. During the acquisition, another golf swing and a tennis backhand were performed. The different tennis movement was not chosen on purpose, as the sensors are expected to give good results independent from the actual movement.

## 5. Results

### 5.3.1. Pelvis: IMUs and marker, IMUs and Shape

It is expected that the sensors have similar correlations compared to day one, as nothing in the setup was changed.

Table 19: Spearman correlation of IM-sensors and marker/silhouette data: Pelvis

| Method            | X       | Y             | Z       | total   |
|-------------------|---------|---------------|---------|---------|
| IMU-marker, $r_s$ | 0,89803 | -0,33340      | 0,98927 | 0,59634 |
| Strength          | strong  | negative weak | strong  | average |
| IMU-Shape, $r_s$  | 0,22260 | 0,52151       | 0,99380 | 0,76298 |
| Strength          | weak    | average-weak  | strong  | average |

*correlations coefficients of Pelvis during golf swing on capture day two*

Although the Z-rotation is correlating strong again, the total correlations are only average.

### 5.3.2. Thorax: IMUs and marker, IMUs and Shape

Table 20: Spearman correlation of IM-sensors and marker/silhouette data: Thorax

| Method            | X       | Y         | Z       | total   |
|-------------------|---------|-----------|---------|---------|
| IMU-marker, $r_s$ | 0,94983 | 0,16314   | 0,98234 | 0,69443 |
| Strength          | strong  | weak-none | strong  | average |
| IMU-Shape, $r_s$  | 0,94806 | 0,26794   | 0,97863 | 0,69768 |
| Strength          | strong  | weak      | strong  | average |

*correlations coefficients of Thorax during golf swing on capture day two*

Again the Z-rotation has a good correlation, but the overall correlations are only average.

### 5.3.3. Upper arm right: IMUs and marker, IMUs and Shape

Table 21: Spearman correlation of IM-sensors and marker/silhouette data: Upper arm right

| Method            | X       | Y         | Z       | total   |
|-------------------|---------|-----------|---------|---------|
| IMU-marker, $r_s$ | 0,72142 | 0,041681  | 0,88214 | 0,75763 |
| Strength          | average | weak-none | strong  | average |
| IMU-Shape, $r_s$  | 0,62404 | 0,06825   | 0,59173 | 0,56336 |
| Strength          | average | weak-none | average | average |

*correlations coefficients of Upper arm right during golf swing on capture day two*

The upper arm right correlations show an even worse overall correlation of the sensors compared to the other two methods. Also the single coordinate correlations are getting weaker.

### 5.3.4. Lower arm right: IMUs and marker, IMUs and Shape

Table 22: Spearman correlation of IM-sensors and marker/silhouette data: Lower arm right

| Method            | X       | Y       | Z       | total     |
|-------------------|---------|---------|---------|-----------|
| IMU-marker, $r_s$ | 0,16422 | 0,84768 | 0,68705 | 0,02117   |
| Strength          | weak    | strong  | average | weak-none |
| IMU-Shape, $r_s$  | 0,43761 | 0,74499 | 0,14917 | 0,29136   |
| Strength          | weak    | average | weak    | weak      |

*correlations coefficients of Lower arm right during golf swing on capture day two*

Although the Y rotations have only had weak correlations and no strong/average, the other values and especially the total correlations get weaker.



## 5. Results

### 5.3.5. Wrist right: IMUs and marker, IMUs and Shape

Table 23: Spearman correlation of IM-sensors and marker/silhouette data: Wrist right

| Method            | X         | Y       | Z       | total   |
|-------------------|-----------|---------|---------|---------|
| IMU-marker, $r_s$ | 0,62367   | 0,90319 | 0,62392 | 0,35941 |
| Strength          | average   | strong  | average | weak    |
| IMU-Shape, $r_s$  | 0,11909   | 0,91368 | 0,52647 | 0,37154 |
| Strength          | weak-none | strong  | average | weak    |

*correlations coefficients of Wrist right during golf swing on capture day two*

When comparing data of the wrist, again the overall correlations are weak.

### 5.4. Tennis backhand capture day two

In the previous section, the overall correlations in the golf swing were only average, getting weaker. So for the second movement which was performed after the golf swing, similar results are expected. The movement performed was a tennis backhand in contrast to the forehand from capture day one.

#### 5.4.1. Pelvis: IMUs and marker, IMUs and Shape

Table 24: Spearman correlation of IM-sensors and marker/silhouette data: Pelvis

| Method            | X       | Y       | Z       | total   |
|-------------------|---------|---------|---------|---------|
| IMU-marker, $r_s$ | 0,82012 | 0,12419 | 0,90541 | 0,81629 |
| Strength          | strong  | weak    | strong  | strong  |
| IMU-Shape, $r_s$  | 0,23063 | 0,14499 | 0,92509 | 0,85985 |
| Strength          | weak    | weak    | strong  | strong  |

*correlations coefficients of Pelvis during golf swing on capture day two*

Compared to the golf swing, also the Tennis backhand features strong correlations concerning the overall data and the Z-data.

## 5. Results

### 5.4.2. Thorax: IMUs and marker, IMUs and Shape

Table 25: Spearman correlation of IM-sensors and marker/silhouette data: Thorax

| Method            | X       | Y       | Z       | total   |
|-------------------|---------|---------|---------|---------|
| IMU-marker, $r_s$ | 0,22229 | 0,55995 | 0,99281 | 0,81463 |
| Strength          | weak    | average | strong  | strong  |
| IMU-Shape, $r_s$  | 0,25130 | 0,66796 | 0,38778 | 0,77551 |
| Strength          | weak    | average | weak    | average |

*correlations coefficients of Thorax during golf swing on capture day two*

Unlike the strong overall correlations in the pelvis, the correlations in the thorax are only average.

### 5.4.3. Upper arm right: IMUs and marker, IMUs and Shape

Table 26: Spearman correlation of IM-sensors and marker/silhouette data: Upper arm right

| Method            | X            | Y       | Z       | total   |
|-------------------|--------------|---------|---------|---------|
| IMU-marker, $r_s$ | 0,40225      | 0,83163 | 0,26392 | 0,77438 |
| Strength          | weak         | strong  | weak    | average |
| IMU-Shape, $r_s$  | 0,51796      | 0,81060 | 0,38279 | 0,72054 |
| Strength          | average-weak | strong  | weak    | average |

*correlations coefficients of Upper arm right during golf swing on capture day two*

The Upper arm right also features in this section average correlations.

#### 5.4.4. Lower arm right: IMUs and marker, IMUs and Shape

Table 27: Spearman correlation of IM-sensors and marker/silhouette data: Lower arm right

| Method            | X       | Y         | Z         | total   |
|-------------------|---------|-----------|-----------|---------|
| IMU-marker, $r_s$ | 0,49364 | 0,09072   | 0,12198   | 0,55807 |
| Strength          | weak    | weak-none | weak      | average |
| IMU-Shape, $r_s$  | 0,32071 | 0,49458   | 0,02281   | 0,45567 |
| Strength          | weak    | weak      | weak-none | weak    |

*correlations coefficients of Lower arm right during golf swing on capture day two*

The data acquired through 'Motion' and 'Shape' correlate even worse with the IMUs concerning the lower arm right.

#### 5.4.5. Wrist right: IMUs and marker, IMUs and Shape

Table 28: Spearman correlation of IM-sensors and marker/silhouette data: Wrist right

| Method            | X       | Y       | Z       | total   |
|-------------------|---------|---------|---------|---------|
| IMU-marker, $r_s$ | 0,76436 | 0,49549 | 0,81177 | 0,75860 |
| Strength          | average | weak    | strong  | average |
| IMU-Shape, $r_s$  | 0,27570 | 0,38756 | 0,90226 | 0,44828 |
| Strength          | weak    | weak    | strong  | weak    |

*correlations coefficients of Wrist right during golf swing on capture day two*

Interestingly the data for the wrist correlates better than Upper and Lower arms.

## 6. Discussion

This section will look at the total correlations of IMUs and markers, to see how close the data is to each other and where there are any problems. Therefore the section will be divided into two sections, the first one talking about similarities in the acquired data of capture day one and day two. The second part will look at a comparison and between the captures of day one and two and try to give an explanation, why during day two, the sensors worked so bad, that the data was impossible to import into Shape.

### 6.1. Total correlations of capture day one and two

In section 4.5, table 3 it was mentioned, that strong correlations are values above 0,8. So when looking at the results of the overall calculated correlations, especially values above 0,8 are of high interest. In the upcoming figures, only the total values are displayed. They were calculated by adding y-,and z-data to the x-data and then calculating Spearman's coefficient from the whole data

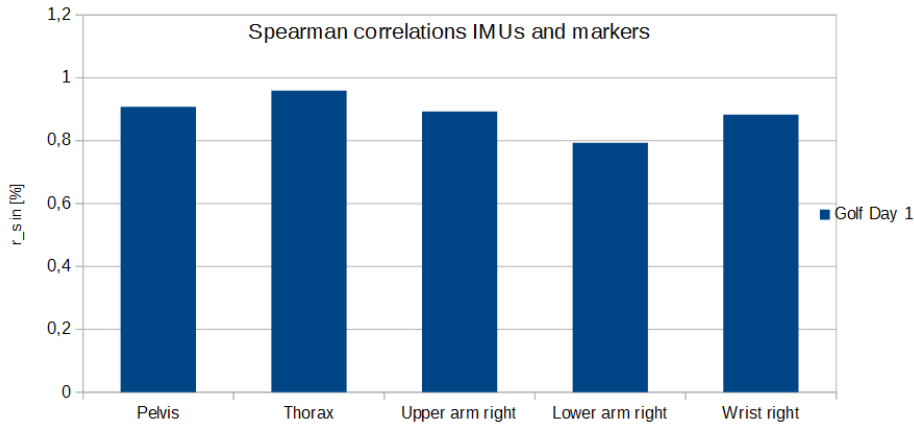


Figure 17: Table with correlation coefficients of total values for golf swing day one

Looking at the figure, it can be noticed, that during this particular golf swing, only the lower arm right has an average-strong correlation (0,79285) while every other body part has strong correlations. A potential cause could be the problem, that the sensors are initialized in the neutral zero position. In this position, the recorded subject should not have any angle in the lower arm, but in this case, there actually was a small angle noticed. Other than that, there is no explanation, that would support this error.

## 6. Discussion

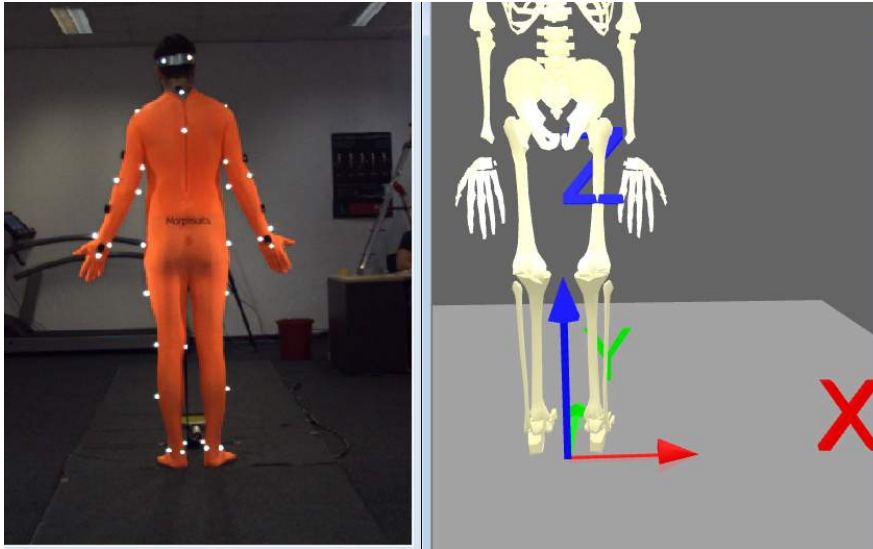


Figure 18: Comparison of lower arms during IMU-initialization: actual position (right) vs. IM-based model (left)

This theory is also supported by the capturing of the tennis forehand on capture day one. During the initialization, the subject also was unable to move its arms in a perfect neutral zero position. Figure 19 shows again, that especially the lower arm right only has an average correlation, while at least the sensors on the upper arm right as well as pelvis and thorax correlate strong. The sensor on the wrist right does also not correlate strong, but at an average of 0,72219. The average is still high and close to a strong value of 0,8. So although the lower arm does not correlate perfectly, the data still shows, that for this capture experiment, IM-sensors do correlate strong to marker data.

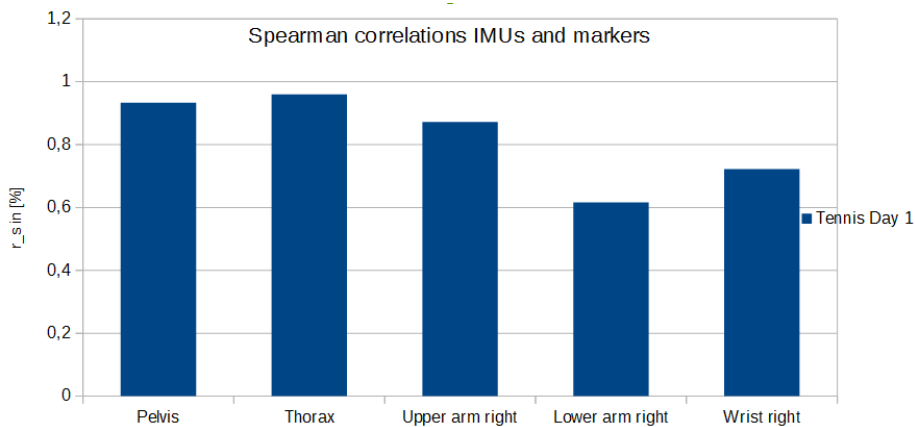


Figure 19: Total correlation coefficients from the tennis forehand on capture day one

As good as the total values of the IMU during the golf swing and tennis forehand

## 6. Discussion

correlated on day one, as bad did they correlate on capture day two. When looking at the data before even calculating the spearman correlation coefficient, the data graphs where totally different from the marker ones and also the IM-inverse kinematics model moved differently from the actual movements. Figure 20 shows that during the golf swing none of the total correlations were better than average, two were even bad or close to no correlation at all.

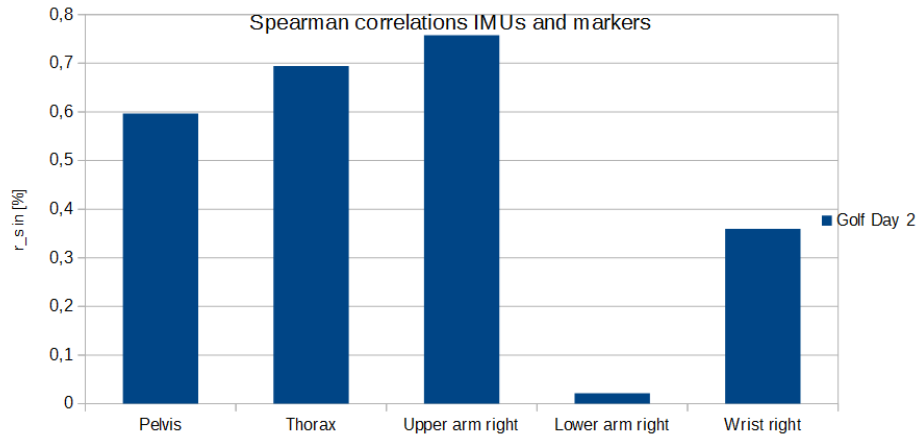


Figure 20: Total correlation coefficients from the golf swing on capture day two

Compared to the golf swing of capture day one, the differences are notable to high. Figure 21 visualizes the differences for each body segment.

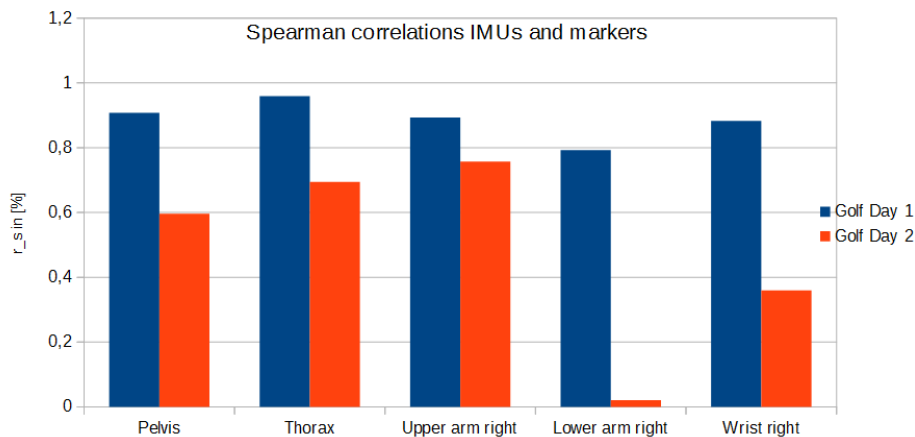


Figure 21: Total correlation coefficients compared from the golf swing on capture days one and two

The problem with this difference is, that nothing was changed at the setup between capture day one and two. Even the exact same sensors were used and placed on almost

## 6. Discussion

the same places of the segments. The only variable that might have changed, is the magnetic field, but as it can not be measured in the laboratory prior to every capture, it is hard to use it as the solution to this problem.

Although the correlations during the tennis backhand are a little better than the ones from the golf swings, both golf swing and backhand were performed in one capture with no re-initialization or pause in between. So the bad captures of day two are inexplicable, especially because the data of day one proves, that the sensors work in a similar way like markers and can also be used to enhance the quality of data, tracked by Shape. Figure 22 shows the comparison of the two tennis movements. Although one is a forehand and one a backhand, the correlation should not differ too much.

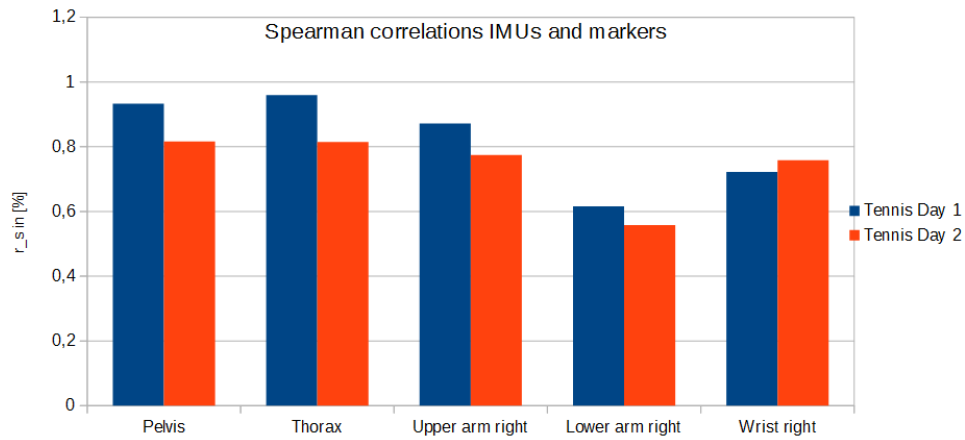


Figure 22: Total correlation coefficients compared from the tennis movements on capture days one and two

# Part III.

## Implementing IMUs into Simi Shape

### 7. Extended Theory

For the implementation of IM-sensor data into Simi's software 'Shape', some additional background information is needed.

#### 7.1. Silhouette tracking in Simi Shape

Other than the already described motion tracking software Simi Motion, 'Shape' only uses silhouette information and therefore is not in need of any retro-reflective markers and ringlights. Instead all cameras only capture the persons silhouette. Data such as calibration and video information is featured from 'Motion'. 'Shape' is only used for tracking and to achieve good tracking results, different aspects concerning the segmentation should be taken into consideration.

- Clear contrast: The subject to be recorded needs to look different from its surroundings. In earlier recordings, a tight fitting morphsuit was used to ensure optimal contrast. For practical reasons, morphsuits are no longer used and so it is important that clothes should have different colors than the floor or walls.
- Close-up picture: cameras should be placed in such a way, that the recorded area features as much movement of the person as possible while featuring only as little movement of anything else as possible.
- light: the area of movement should be as bright as possible. When using Shape in combination with markers, direct light like windows make it impossible to track markers good. As this was the case in the thesis only passive light was used. For captures with Shape solely, cameras are also allowed to face windows and direct light can be used.

The process of markerless tracking can be divided into three major steps. First the segmentation is performed, using two kinds of videos: the actual movement and an empty image recorded without anybody inside the movement area. To get good segmentation, the empty image has to match the image of the movement in terms of light, color and



objects. The software compares color of every pixel of every camera during this step. If the upper threshold of at least one color channel is too high, the pixel is associated with the recorded subject. Also if the lower threshold of at least one color channel is too low, the pixel is not seen as background anymore. The same happens to different light settings or objects that appear only in one of the videos. Another option features a solution to captures, that are performed during training sessions. If during those sessions, the applicant walks out of the starting position, the background can also be subtracted by means of creating a new background. This solution is applicable especially for sessions, where the light changes too much or there is no time for recording a background video.

Step two is the model initialization or model fitting. In this process, a mathematical model is fitted into the silhouette of the subject. The better step one was executed, the better the model fits. In general a Psi-pose is used for this initialization but the pose can be adopted manually if, for example the subject is running into the image or like in a training session has no time to perform a certain pose. During model initialization the model is fitted exactly as the subject is positioned. This does not only include position of body parts but also height and proportions of the segments.

Step three is the last step and consists of the actual tracking itself. Once the model is fitted into the silhouette, the tracking process can be started and the recorded movement will be performed. In every single frame of the movement, the model is fitted into the subject's silhouette. An iteration setting can be adopted to calculate on slow movements faster or optimize its pose more often during fast movements. If the silhouette is lost during the tracking process, the tracking can be paused and the model readjusted. After finished tracking, the data can be exported in form of joint centers, joint angles and an inverse kinematics folder. This also includes segment rotations.

The model used is the same like in 'Motion' with the difference, that lower legs and arms are only connected to the upper arms (upper legs respectively) through hinge joints. Those joints do not allow the lower arm to rotate radius around ulna. [6, p.13, 29, 56, 69]

### **7.1.1. Implementing IMUs into marker-less tracking Simi Shape**

Although 'Shape' only functions as an add-on for marker-less tracking, IM-sensor based data needs to be implemented, too. The only difference is, that when imported into 'Shape', the IM-rotations are already transformed into the global L-frame-coordinate system and zero set on the segments they are attached to. So the rotations imported into 'Shape' are already transformed onto the segments and need no further calculation.

## 7. Extended Theory

With this rotational data, there still is one problem in 'Shape'. The data contains information about the rotations performed by the subject but neither does it consist the actual placement (orientation) of the sensor nor the offset of the segment towards the global L-frame-coordinate system. So to assign the right rotation data to the right segment, it has to be transformed into the segment-local-coordinate system. This transformation does not work like an actual calculation like the transformations in 'Motion' but is performed via certain steps. Those steps are described in further detail in the 'Methods' section of this part.

Unlike 'Motion', 'Shape' is not used for marker- or IMU-tracking solely, so the information imported from markers or IM-sensors is only used to support certain segments in their tracking process. One example is the pelvic joint, which is connected via a ball joint to the trunk and can therefore move differently from the human hip. Especially because the body of a shape model only consists of the trunk and the hip, spinal rotations will be translated into rotations of hip and thorax only. This can cause problems, when the hip tries to fit into the silhouette but should actually rotate in a different way. Figure 23 shows such a problem

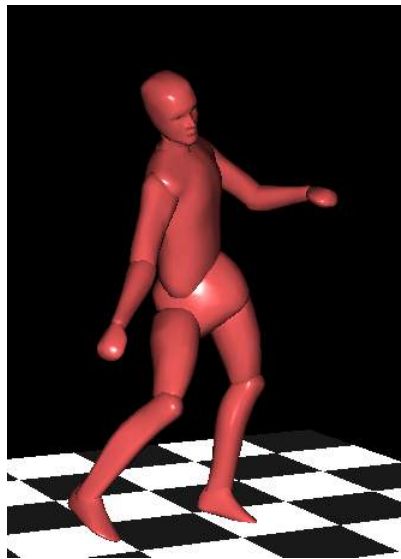


Figure 23: tilted hip during tennis forehand movement

Another problem is the inversion/eversion of the arm. Although the arm rotates, the silhouette does hardly change, therefore the software does not know for sure, which way the arm is rotated. The problem that can happen is, that the arm is rotated in a impossible way and when the movement gets to a point, where the model's arm can no longer be fitted into the silhouette, a conflict appears. In case of Figure 24, the lower

## 8. Additional Methods

arm could no longer be fitted into its assigned silhouette and is moved into the upper arm. That way it is ensured that the upper arm can still be fitted correctly. The arm can be refitted in a paused tracking process but it does not solve the problem itself. One possible solution to those problems is to support the tracking with rotational information from markers or IM-sensors.

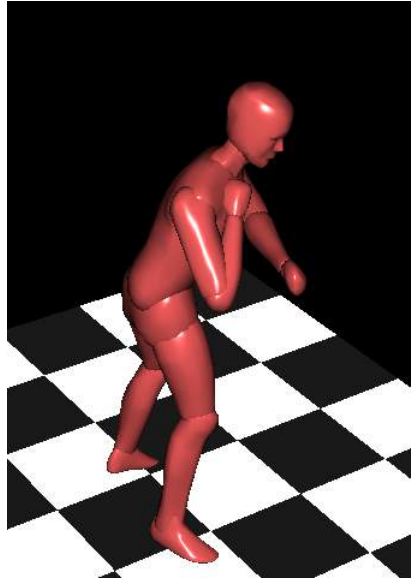


Figure 24: tilted arm during golf pre-swing phase movement

## 8. Additional Methods

This section will only feature methods different from the ones mentioned in the previous part.

### 8.1. marker-less tracking

Simi Shape uses all video files, loaded into 'Motion' for further tracking. To achieve good tracking results, it was mentioned in an earlier section, that the segmentation has to be good. Therefore the movement video files have to be bright and clear enough, to see a the recorded subject in the image. This is not always the case, as many fast movements not only have to be recorded at a high frequency, but also the exposure time has to be low. Otherwise the image will appear blurry during the fast movements and 'Shape' will no longer 'know' at what exact position the arm is placed. A negative side-effect of a low exposure time is a dark video image which in this form is not any good for

silhouette tracking. The process to edit the recorded video file post-capture is called image processing or 'image-pipe'. In this editing, the video can be brightened up and also contrast and gamma of the picture can be changed. With the edited settings, the video can then be imported into 'Shape' and used for tracking.

Another important issue is the video used for background subtraction. Like written in the section above, 'Shape' uses a background video, also called empty image, to evaluate, which parts of the movement video are parts of the subject and which are parts of the background. Not only objects count but also video image brightness, contrast and color. So if an empty image is recorded previously to capturing, the light settings and also the post-capture image processing has to be the exact same like the movement video. In other words, the image settings in both empty image and movement video have to be the same.

For the means of the empty image, there are two ways to record them using background subtraction: either an empty image of 1-2 seconds is recorded previously to movements or at every time in between different movements if any of the room-settings change. The second way is to record the empty image right at the beginning of the movement, meaning the recorded subject will have to stand outside the room and then 1-2 seconds into the video, he/she will walk in and do his/her movement. The recorded videos will then be saved as 2D-calibration files and movement videos at the same time. In this case, one empty image recording was done for each capture day, so that the subject was able to start its 20 seconds of neutral-zero positioning for the IM-sensor initialization standing in the exact are of movement and not having to walk through different sets magnetic fields to record its movement.

Prior to video import into 'Shape', the changed image settings were exported into the actual video-file, to ensure, that 'Shape' uses the right settings. Tracking and data export back into 'Motion' as well as data preparation was mentioned already and will to no further extend be written about.

### 8.2. hybrid marker-based tracking

Like IM-sensors based tracking and silhouette-tracking is compared to marker tracking being the gold-standard, another method is introduced in this thesis as well. In order to compare hybrid-IM based tracking not only with silhouette tracking solely, a hybrid silhouette-marker based tracking is also used. For this specific method, certain markers from the inverse kinematics marker model are used. Those are:

## 8. Additional Methods

- Hip/Pelvis: three markers are used to support the hip, mid spina iliaca posterior and spina iliaca anterior superior left and right. Data from those three markers will create the pelvis-model
- Thorax: four markers are used to support the thorax/ upper body, manubrium sterni, C7 as well as Acromion left and right. The thorax model can be created from this.
- Upper arm: three markers are used to support the upper arm, Acromion right, right biceps lateralis and right triceps lateralis.
- Wrist right: wrist medialis right and lateralis right as well as middle finger base joint are the three markers for this segment.

The lower arm is not supported in the setup, because like mentioned in section 7.1.1., the 'Shape'-model does not differentiate between upper and lower arm rotations. This is because the elbow just serves as a hinge joint but is not made for rotations of ulna around radius. So if such a rotation is imported in 'Shape', it will lead to conflicts in tracking. Therefore the lower arm is left out.

In order to import 3D-data from 'Motion', the data just has to be selected in the menu and some settings have to be changed. In the menu 'Marker settings' the data from the wanted segments has to be selected and then implemented Shape-model-markers are initialized at the actual 3D-position. Another important setting is the weight of which the data is used compared to the silhouette data. L.Becker found out that the optimal weight is silhouette weight being twenty times higher than marker weight, so the marker weight was set to 0.05 compared to 1.00 for silhouette weight. Once everything is set, the markers will appear as yellow dots on the Shape-model.

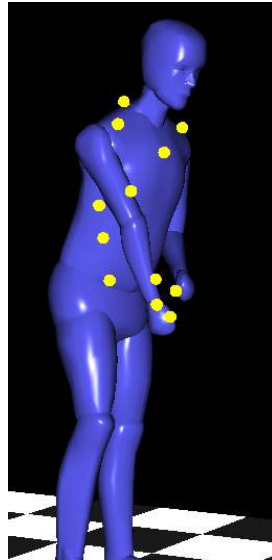


Figure 25: Initialized markers on Shape-model for hybrid marker-based silhouette tracking

Tracking and data export is same to solely silhouette tracking.

### 8.3. hybrid IMU-based tracking

Like hybrid marker tracking, IMU-based hybrid tracking also uses data sets exported from 'Motion'. One difference is, that IM-sensor data first has to be applied to a certain model. This happens when selecting the 'apply rotations to model'-option and then dragging the sensors to the segments, on which they were placed on. Afterwards the rotational data can be selected like marker 3D-data in 'Shape'. In the Rotations settings various things have to be selected to make the sensors data usable in 'Shape' as well.

- Selecting the right data: once imported, the segment-assigned sensors can be selected in a list. All other body-segments are grayed out and can not be activated.
- Local coordinate systems: once selected, small sensor coordinate axes appear on the model, where the sensors where placed. Red shows the X-axis, green the Y-axis and blue the Z-axis, respectively. The coordinate systems will appear inside the joints, where the segments are connected to each other so the wrist coordinate system is actually placed in the wrist joint, lower arm in the elbow, et cetera [etc.]. One special case are the coordinate systems of pelvis and thorax, as both appear in the connection of pelvis and thorax.

## 8. Additional Methods

- **Coordinate transformation:** when selecting the sensor offsets, the current offsets of the sensors compared to the global L-frame-coordinate system will be shown. To set those offsets to zero, the sensor offsets can be turned by moving the X-, Y- and Z-value-bars to the position, they were positioned during the first offset-measurement in the sensor calibration. In this case the sensors were placed like the L-frame, with X, Y and Z aligned to X, Y and Z of the L-frame coordinate system. Therefore one sensors offset-coordinate system has to be turned to match the L-frame. In a second step, the sensors offset from the global coordinate system to the segments local system can be calculated by clicking 'set world coordinate system'. The offset is then calculated automatically. By selecting 'align sensors' the offset of the current sensor will be used to calculate the orientation of all other sensors. If the data is right, all sensors offset-coordinate systems should then be aligned with the global L-frame system.
- **Weighing:** Like 3D-marker correspondences, IMU-based rotations also have to be weighed against silhouette-based information. Various trials show, that the marker settings work for the IMU-settings, too. So IM-correspondences are also set to 0.05.

Again, no lower arm data is imported, because it causes conflicts in the rotations of the lower arm compared to the upper arm. The same conflict would also appear in the lower leg, as it is also only connected through a hinge joint to the upper leg, too.



Figure 26: IM-sensor settings in 'Shape' X=red, Y=green, Z=blue

Unlike marker-based hybrid tracking, IM-sensor hybrid tracking is not always too

## 9. Results

stable, so it could happen, that after time, the silhouette is lost and the model vanished due to too many conflicts. In this case, the tracking has to be stopped and the model reset.

## 9. Results

Regarding the Results of this second section, it has to be said, that the data groups correlated differ from part one. As part one solely focused on the implementation of the sensors in Simi Motion and then comparing it with Marker data and Shape data, this section will feature groups from two different hybrid trackings. On one hand, hybrid tracking data of markers supporting Shape will be correlated to marker data. On the other hand, hybrid tracking data of IM sensors supporting Shape will be correlated to marker data again. In a third comparison, hybrid IM sensor data will be correlated to hybrid marker data.

Sections 5.3 and 5.4 already showed, that concerning capture day two, IM sensor data did not correlate strongly enough to either marker or silhouette data. Therefore, it made no sense to take the different data files from the sensors and integrate them into Shape. In a practical try, this idea failed and no data could be tracked. So in the sub-section of capture day two, there is no hybrid sensor data and can thus not be compared to hybrid marker and solely marker data.

### 9.1. Golf swing capture day one

#### 9.1.1. Pelvis: Hybrid marker-Shape and hybrid IMU-Shape

Table 29: Spearman correlation of hybrid silhouette data: Pelvis

| Method                         | X       | Y       | Z       | total   |
|--------------------------------|---------|---------|---------|---------|
| marker-shape and marker, $r_s$ | 0,96011 | 0,68008 | 0,71319 | 0,92081 |
| Strength                       | strong  | average | average | strong  |
| IMU-Shape and marker, $r_s$    | 0,91088 | 0,85934 | 0,93223 | 0,93369 |
| Strength                       | strong  | strong  | strong  | strong  |

*Hybrid correlations coefficients of Pelvis during golf swing on capture day one*



## 9. Results

### 9.1.2. Thorax: Hybrid marker-Shape and hybrid IMU-Shape

Table 30: Spearman correlation of hybrid silhouette data: Thorax

| Method                         | X       | Y            | Z       | total   |
|--------------------------------|---------|--------------|---------|---------|
| marker-shape and marker, $r_s$ | 0,96423 | 0,92926      | 0,91765 | 0,98086 |
| Strength                       | strong  | strong       | strong  | strong  |
| IMU-Shape and marker, $r_s$    | 0,88582 | 0,50829      | 0,94687 | 0,96816 |
| Strength                       | strong  | average-weak | strong  | strong  |

*Hybrid correlations coefficients of Thorax during golf swing on capture day one*

Despite an average correlation of the Pelvis hybrid marker data, concerning the Thorax, the data of both hybrid tracking methods show strong correlations

### 9.1.3. Upper arm right: Hybrid marker-Shape and hybrid IMU-Shape

Table 31: Spearman correlation of hybrid silhouette data: Upper arm right

| Method                         | X       | Y       | Z       | total   |
|--------------------------------|---------|---------|---------|---------|
| marker-shape and marker, $r_s$ | 0,96794 | 0,94967 | 0,94034 | 0,97946 |
| Strength                       | strong  | strong  | strong  | strong  |
| IMU-Shape and marker, $r_s$    | 0,94358 | 0,96809 | 0,92662 | 0,96141 |
| Strength                       | strong  | strong  | strong  | strong  |

*Hybrid correlations coefficients of Upper arm right during golf swing on capture day one*

The upper arm right shows, how close both hybrid tracking methods correlate to the marker gold-standard.

## 9. Results

### 9.1.4. Lower arm right: Hybrid marker-Shape and hybrid IMU-Shape

Table 32: Spearman correlation of hybrid silhouette data: Lower arm right

| Method                         | X       | Y       | Z       | total   |
|--------------------------------|---------|---------|---------|---------|
| marker-shape and marker, $r_s$ | 0,94293 | 0,94813 | 0,9621  | 0,81542 |
| Strength                       | strong  | strong  | strong  | strong  |
| IMU-Shape and marker, $r_s$    | 0,77131 | 0,87533 | 0,53281 | 0,63971 |
| Strength                       | average | strong  | average | average |

*Hybrid correlations coefficients of Lower arm right during golf swing on capture day one*

### 9.1.5. Wrist right: Hybrid marker-Shape and hybrid IMU-Shape

Table 33: Spearman correlation of hybrid silhouette data: Wrist right

| Method                         | X       | Y       | Z       | total   |
|--------------------------------|---------|---------|---------|---------|
| marker-shape and marker, $r_s$ | 0,39010 | 0,91489 | 0,82328 | 0,41852 |
| Strength                       | weak    | strong  | strong  | weak    |
| IMU-Shape and marker, $r_s$    | 0,17884 | 0,54456 | 0,19456 | 0,16088 |
| Strength                       | weak    | average | weak    | weak    |

*Hybrid correlations coefficients of Wrist right during golf swing on capture day one*

## 9.2. Tennis forehand capture day one

### 9.2.1. Pelvis: Hybrid marker-Shape and hybrid IMU-Shape

Table 34: Spearman correlation of hybrid silhouette data: Pelvis

| Method                         | X       | Y       | Z       | total   |
|--------------------------------|---------|---------|---------|---------|
| marker-shape and marker, $r_s$ | 0,97428 | 0,24506 | 0,95646 | 0,95329 |
| Strength                       | strong  | weak    | strong  | strong  |
| IMU-Shape and marker, $r_s$    | 0,96485 | 0,45116 | 0,95260 | 0,95940 |
| Strength                       | strong  | weak    | strong  | strong  |

*Hybrid correlations coefficients of Pelvis during tennis forehand on capture day one*

It is interesting to see how close the correlations of both marker-shape data and IMU-shape data come to each other. They barely differ.

## 9. Results

### 9.2.2. Thorax: Hybrid marker-Shape and hybrid IMU-Shape

Table 35: Spearman correlation of hybrid silhouette data: Thorax

| Method                         | X       | Y       | Z       | total   |
|--------------------------------|---------|---------|---------|---------|
| marker-shape and marker, $r_s$ | 0,99483 | 0,97852 | 0,97720 | 0,99534 |
| Strength                       | strong  | strong  | strong  | strong  |
| IMU-Shape and marker, $r_s$    | 0,99427 | 0,97554 | 0,95260 | 0,99342 |
| Strength                       | strong  | strong  | strong  | strong  |

*Hybrid correlations coefficients of Thorax during tennis forehand on capture day one*

Again, both hybrid methods correlate with each other very close.

### 9.2.3. Upper arm right: Hybrid marker-Shape and hybrid IMU-Shape

Table 36: Spearman correlation of hybrid silhouette data: Upper arm right

| Method                         | X       | Y       | Z       | total   |
|--------------------------------|---------|---------|---------|---------|
| marker-shape and marker, $r_s$ | 0,96254 | 0,94185 | 0,90615 | 0,98067 |
| Strength                       | strong  | strong  | strong  | strong  |
| IMU-Shape and marker, $r_s$    | 0,98621 | 0,95648 | 0,91118 | 0,98506 |
| Strength                       | strong  | strong  | strong  | strong  |

*Hybrid correlations coefficients of Upper arm right during tennis forehand on capture day one*

### 9.2.4. Lower arm right: Hybrid marker-Shape and hybrid IMU-Shape

Table 37: Spearman correlation of hybrid silhouette data: Lower arm right

| Method                         | X       | Y       | Z       | total   |
|--------------------------------|---------|---------|---------|---------|
| marker-shape and marker, $r_s$ | 0,73446 | 0,98114 | 0,27174 | 0,36397 |
| Strength                       | average | strong  | weak    | weak    |
| IMU-Shape and marker, $r_s$    | 0,73253 | 0,96121 | 0,27229 | 0,34155 |
| Strength                       | average | strong  | weak    | weak    |

*Hybrid correlations coefficients of Lower arm right during tennis forehand on capture day one*

## 9. Results

Although both methods do not correlate very good to the marker data, again, they correlate good to each other.

### 9.2.5. Wrist right: Hybrid marker-Shape and hybrid IMU-Shape

Table 38: Spearman correlation of hybrid silhouette data: Wrist right

| Method                         | X         | Y       | Z       | total   |
|--------------------------------|-----------|---------|---------|---------|
| marker-shape and marker, $r_s$ | 0,29727   | 0,84979 | 0,46950 | 0,25099 |
| Strength                       | weak      | strong  | weak    | weak    |
| IMU-Shape and marker, $r_s$    | 0,06159   | 0,86811 | 0,94809 | 0,19655 |
| Strength                       | weak-none | strong  | strong  | weak    |

*Hybrid correlations coefficients of Wrist right during tennis forehand on capture day one*

## 9.3. Golf and Tennis capture day two

As mentioned above, data from the IM-sensors compared to shape and markers did only correlate on average or weak basis. Therefore a hybrid tracking including the IM-sensors was chosen not to perform. Thus this section will only compare shape based data with hybrid marker-shape data for the golf swing and the tennis backhand together.

### 9.3.1. Pelvis: Hybrid marker-Shape and marker for golf and tennis backhand

Table 39: Spearman correlation of hybrid silhouette data: Pelvis

| Method                               | X       | Y       | Z       | total   |
|--------------------------------------|---------|---------|---------|---------|
| marker-shape and Shape golf, $r_s$   | 0,90107 | 0,94820 | 0,97987 | 0,96017 |
| Strength                             | strong  | strong  | strong  | strong  |
| marker-shape and Shape tennis, $r_s$ | 0,94590 | 0,63015 | 0,42196 | 0,93797 |
| Strength                             | strong  | average | weak    | strong  |

*Hybrid correlations coefficients of Thorax during tennis and golf on capture day two*

9. Results

**9.3.2. Thorax: Hybrid marker-Shape and marker for golf and tennis backhand**

Table 40: Spearman correlation of hybrid silhouette data: Thorax

| Method                               | X       | Y       | Z       | total   |
|--------------------------------------|---------|---------|---------|---------|
| marker-shape and Shape golf, $r_s$   | 0,96669 | 0,74660 | 0,98014 | 0,97949 |
| Strength                             | strong  | average | strong  | strong  |
| marker-shape and Shape tennis, $r_s$ | 0,97533 | 0,75056 | 0,94807 | 0,97601 |
| Strength                             | strong  | average | strong  | strong  |

*Hybrid correlations coefficients of Thorax during tennis and golf on capture day two*

**9.3.3. Upper arm right: Hybrid marker-Shape and marker for golf and tennis backhand**

Table 41: Spearman correlation of hybrid silhouette data: Upper arm right

| Method                               | X       | Y       | Z       | total   |
|--------------------------------------|---------|---------|---------|---------|
| marker-shape and Shape golf, $r_s$   | 0,94671 | 0,99153 | 0,92270 | 0,97804 |
| Strength                             | strong  | strong  | strong  | strong  |
| marker-shape and Shape tennis, $r_s$ | 0,98543 | 0,97347 | 0,94491 | 0,99037 |
| Strength                             | strong  | strong  | strong  | strong  |

*Hybrid correlations coefficients of Upper arm right during tennis and golf on capture day two*

**9.3.4. Lower arm right: Hybrid marker-Shape and marker for golf and tennis backhand**

Table 42: Spearman correlation of hybrid silhouette data: Lower arm right

| Method                               | X       | Y       | Z       | total   |
|--------------------------------------|---------|---------|---------|---------|
| marker-shape and Shape golf, $r_s$   | 0,81209 | 0,99895 | 0,92793 | 0,81326 |
| Strength                             | average | strong  | strong  | average |
| marker-shape and Shape tennis, $r_s$ | 0,97220 | 0,87030 | 0,82511 | 0,98877 |
| Strength                             | strong  | average | average | strong  |

*Hybrid correlations coefficients of Lower arm right during tennis and golf on capture day two*

### 9.3.5. Wrist right: Hybrid marker-Shape and marker for golf and tennis backhand

Table 43: Spearman correlation of hybrid silhouette data: Wrist right

| Method                               | X        | Y         | Z       | total   |
|--------------------------------------|----------|-----------|---------|---------|
| marker-shape and Shape golf, $r_s$   | 0,835947 | 0,92654   | 0,77557 | 0,77378 |
| Strength                             | average  | strong    | average | average |
| marker-shape and Shape tennis, $r_s$ | 0,50830  | 0,01410   | 0,27456 | 0,60473 |
| Strength                             | average  | weak-none | weak    | average |

*Hybrid correlations coefficients of Wrist right during tennis and golf on capture day two*

## 10. Discussion

This section will focus on the comparison of hybrid marker-shape data and hybrid IMU-shape data from capture day one (each correlated to markers). Also the correlation of both hybrid methods will be featured. In addition to that, hybrid marker-shape data from both day one and two will be looked at. Like mentioned previously, there is no data of any hybrid IMU-shape data from day two, therefore they will not be discussed to any further detail.

One thing that comes straight to the mind is the fact, that the correlation data of hybrid IMU data and hybrid marker data has strong values in both pelvis and thorax, but also in the upper arm. Figures 27. and 28. show, that during the golf swing and the tennis forehand of day one, hybrid IMU data and hybrid marker data is almost the same. While Upper arm right and thorax / pelvis data correlates in strong values in both sport movements, lower arm right and wrist have only strong-average and weak correlations. That is due to the fact, that during normal Shape-tracking, both wrists are locked and can not be moved in order to prevent incorrect wrist rotations. It was proven in previous trackings, that the wrists track even worse, if they are unlocked. So when this data is supported by marker data, it obviously looks different from the original data.

For the IM-sensor data the reason for weak correlations is different. It was mentioned before, that the sensors need an initializing pose in the neutral zero position. The problem with this position was already mentioned, to be hard to fit the lower arms and wrists in the actual position. So this might be an answer, why the solutions correlate only average to weak. Another option is the fact, that especially during golf- and tennis-

## 10. Discussion

movements, both lower arms and wrist are located the furthest away from the original calibrated space. This space is in the exact position, where the movement will happen to prevent differences in the magnetic field and get as close to the exact data, as possible. As lower arm and wrist are the furthest away, they might also be a victim to small magnetic field changes and the data might not be exact anymore. However this is only an assumption based on different measurements.

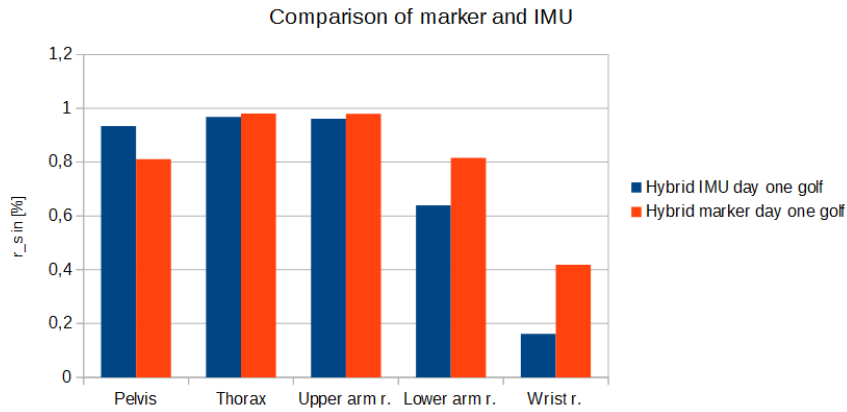


Figure 27: Total correlation coefficients from hybrid-marker and -imu data during golf swing on day one

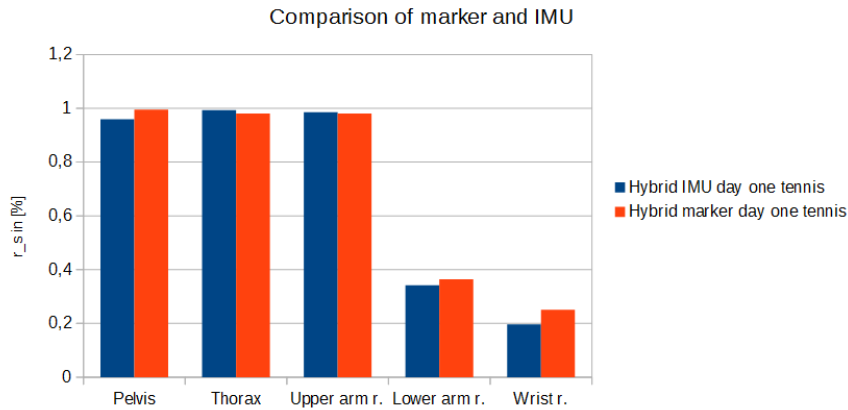


Figure 28: Total correlation coefficients from hybrid-marker and -imu data during tennis forehand on day one

When comparing both hybrid-methods with each other, the correlations are strong in almost every value. Again a problem is the wrist, that sometimes for no particular reason the IM-sensor hybrid version correlates better than the marker hybrid method.

## 10. Discussion

Therefore for both the tennis and the golf movement have weak correlations concerning the wrist. Figure 29. compares golf swing and tennis forehand.

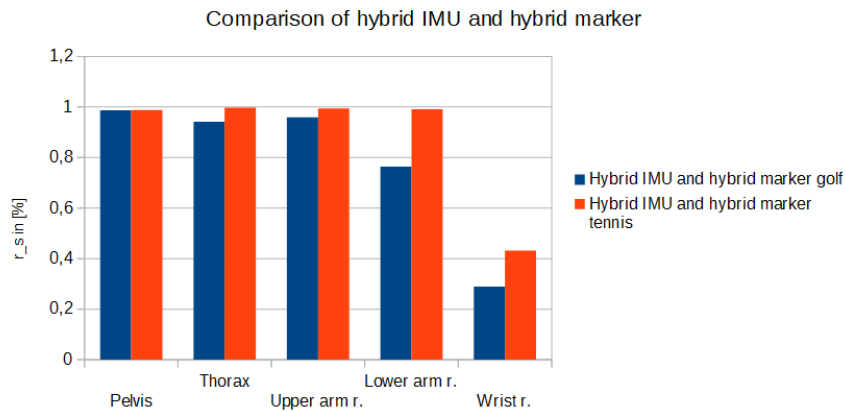


Figure 29: Total correlation coefficients from hybrid-marker and -imu data during golf and tennis forehand on day one

### 10.1. Comparison of hybrid marker-shape data of capture day two

Although the sensors did not give any reasonable data for capture day two, there are some data to be compared to when talking about hybrid tracking in Shape: the hybrid-marker shape data. In this subsection, both total correlation coefficients from the golf swing and the tennis forehand / backhand of day one and two can be looked at, to see in which cases there is consistency and in which there is not. Again pelvis, thorax and upper arm right have strong correlations during both movements, regardless which movement was performed. For the golf swing, the data was average-strong and strong in all cases during capture day two, while during day one, the lower-arm right was correlating on an average-weak value. This could be, because there were some mistakes performed during marker tracking or some markers not tracked the right way.

For the tennis forehand and backhand again the data from captured day two is better in all segments compared to day one. Like during the golf-swing, the tennis movement might not have been tracked perfectly or some mistakes performed during automatic tracking. In addition to that, there is another theory, why the correlations in wrist and lower arm right are only average and weak. The theory is, that during both captures two different kind of movements were performed, the forehand and the backhand. The theory now is, that during the forehand (especially during the reach back), not all markers could



## 10. Discussion

be seen in two cameras and had to be splined to get 3D-data during every single frame. During the backhand though, it was easier to track the hand with the racket in always at least two cameras and produce more accurate data. Figures 30. and 31. show the results, discussed in this subsection.

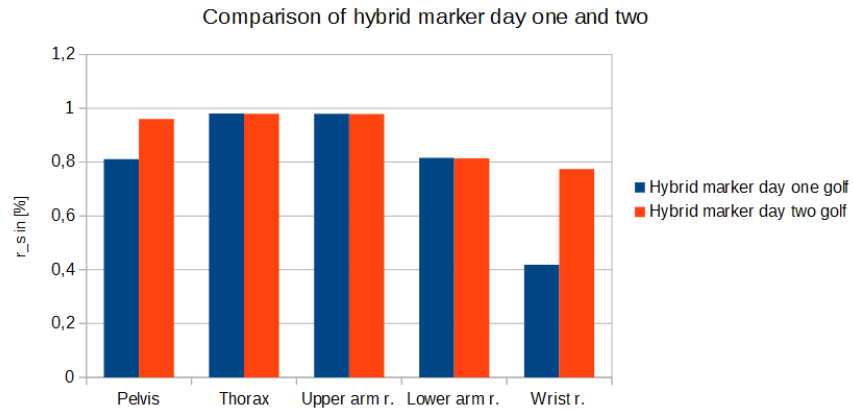


Figure 30: Total correlation coefficients from hybrid-marker data during golf swing day one and two

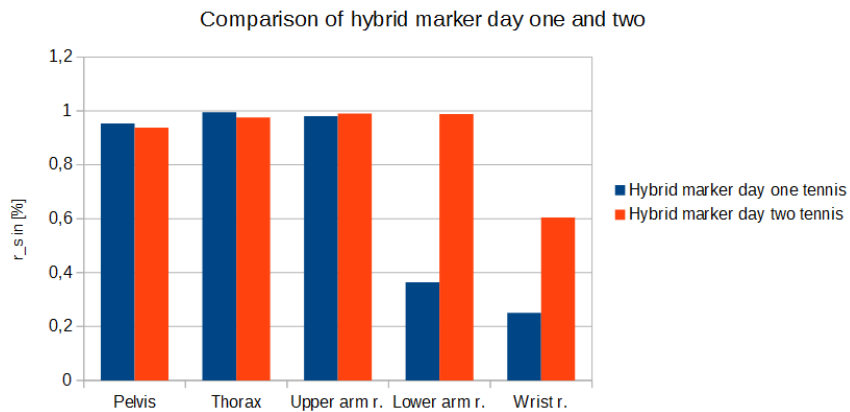


Figure 31: Total correlation coefficients from hybrid-marker data during tennis forehand / backhand on day one and two

# Part IV.

## Conclusion

To conclude this thesis, several points have to be taken into consideration.

To begin with, the original aim of the thesis was to check, if and how IM-sensors can be integrated into marker-based and marker-less 3D-motion tracking. This method was then validated by two different sports-movements: a golf swing and a tennis fore-hand/backhand. Both movements were recorded on different dates to see, if the acquired data is consistent.

The aim to integrate the sensors into marker-based and marker-less 3D-tracking was achieved by finding a solution to various sensor-based problems. Those included different undefinable Z-offsets and coordinate-transformations from IM-sensor coordinate systems into Simi's software Motion and further-on into Shape. The inconsistency of the offsets due to the magnetic field could not be solved, but as the movements were recorded in the same place, no solution was needed for this particular set-up. Other movements such as running or in general movements through a larger space will face this problem nevertheless.

The validation of the sensors' data-output resulted in two different findings.

1. Data from the capture of day one shows, that if the sensors work fine, the sensor data can be taken to replace marker data and therefore use their rotations to enhance marker-less silhouette tracking. Also the sensors can be used solely to get data from certain movements without camera-based tracking. Both golf and tennis movements have average-strong to strong correlations.
2. Data from the capture of day two shows, that although the set-up remained the same, good results are not consistent. Weak to no correlations of IM-sensors to markers show, that the sensors do not always work fine and therefore were not integrated into Shape during capture two. This resulted in the lack of data to compare hybrid marker-Shape data with hybrid IMU-Shape data. Reasons for this bad behavior is likely to be the inconsistency of the magnetic field, which changes are hardly impossible to measure in every-day laboratory set-ups.

Summing up the conclusion of the thesis is split in half. On one hand a possible integration into marker-based and marker-less 3D-tracking was found and if the sensors work fine, acquired data can be used to support silhouette-tracking. On the other hand,

if the sensors do not work fine, it is impossible to integrate the sensors, as the data is not correlating to the marker- or shape-data. One possible cause is the inconsistent magnetic field, which can not be determined and then eradicated in every-day captures. Captures with IM-sensors have to be treated with suspicion, if exact data is required.

## References

- [1] Simi Reality Motion Systems GmbH, *Motion Benutzerhandbuch Version 9.1.1*. Max-Planck-Strasse 11, DE-85716 Unterschleissheim, 2015. original version published in German.
- [2] Wikipedia, “Body planes,” 2016. <https://en.wikipedia.org/wiki/File:BodyPlanes.jpg>.
- [3] OpenStax College, “Types of synovial joints.” Anatomy and Physiology, Connexions Web site., 2013. <http://cnx.org/content/col11496/1.6/>.
- [4] Jutta Merten, “Bewegungsrichtungen,” 2016. <http://www.muskelaufbauforum.de/planer/Bewegungen.jpg>.
- [5] RP Kuster, “Accuracy of kinectone to quantify kinematics of the upper body..” pubmed, 2016. <http://www.ncbi.nlm.nih.gov/pubmed/27264408>.
- [6] Simi Reality Motion Systems GmbH, *Simi Shape User Manual*. Simi Reality Motion Systems GmbH, Max-Planck-Straße 11 DE-85716 Unterschleißheim, May 2015. p.21.
- [7] Linda Becker, “Evaluation of joint angle accuracy using markerless silhouettebased tracking and hybrid tracking against traditional marker tracking,” Master’s thesis, Otto-von-Guericke-Universität Magdeburg, 2016.
- [8] Patrick Stakem, *The History of Spacecraft Computers from V-2 to the Space Station*. PRB publishing, 2010. ASIN B004L626U6.
- [9] “Inertial navigation system.” Wikipedia, June 2016. [https://en.wikipedia.org/wiki/Inertial\\_navigation\\_system](https://en.wikipedia.org/wiki/Inertial_navigation_system).
- [10] Simi Reality Motion Systems GmbH, *Motion - Guideline to conduct a Gait analysis with Simi Motion*. Max-Planck-Strasse 1 DE-85716 Unterschleissheim, 2015.
- [11] David A. Winter, *The Biomechanics and Motor Control of Human Gait*. Waterloo, Canada: University of Waterloo Press, 1987.
- [12] Alexander L. Bell, Douglas R. Pedersen, Richard A. Brand, “A comparison of the accuracy of several hip center location prediction methods,” *Journal of Biomechanics*, vol. 23, no. 6, pp. 617–625, 1990.
- [13] Paolo de Leva, “Joint centers longitudinal positions from a selected subset of chandler’s data,” *Journal of Biomechanics*, vol. 29, pp. 1231–1233, September 1996.
- [14] Aerostudents.com, “Basic principles of inertial navigation seminar on inertial navigation systems,” tech. rep., Tampere University of Technology, 2015. [aerostudents.com/files/avionics/InertialNavigationSystems.pdf](http://aerostudents.com/files/avionics/InertialNavigationSystems.pdf).

- [15] Prof. Dr.-Ing. Jörg Buchholz, *Regelungstechnik und Flugregler Vorlesungsmanuskript*. München: GRIN Verlag, 2010.
- [16] Delsys, *Trigno<sup>TM</sup> SDK Server Reference Guide*. Delsys, 23 Strathmore Road, Natick, MA, 01760 USA. unpublished.
- [17] Delsys, *Trigno<sup>TM</sup> IM Sensor*. Delsys, 23 Strathmore Road, Natick, MA, 01760 USA. [www.delsys.com/Attachments\\_pdf/product-sheets/Trigno-IM.pdf](http://www.delsys.com/Attachments_pdf/product-sheets/Trigno-IM.pdf).
- [18] Dr. Lothar Papula, *Mathematische Formelsammlung für Ingenieure und Naturwissenschaftler*. Wiesbaden: Vieweg + Teubner GWV Fachverlage GmbH, 2009.
- [19] Fernuni Hagen, "Korrelationskoeffizient." [http://www.fernuni-hagen.de/ksw/neustatistik/content/MOD\\_23196/html/comp\\_23414.html](http://www.fernuni-hagen.de/ksw/neustatistik/content/MOD_23196/html/comp_23414.html). letzter Zugriff: 02.07.2016.
- [20] medistat GmbH, "Rangkorrelationskoeffizient nach spearman." <https://www.medistat.de/glossar/korrelation-assoziation/rangkorrelationskoeffizient-nach-spearman>. Zuletzt zugegriffen am 02.07.2016.
- [21] J. Richards, *Biomechanics in clinic research*. Churchill Livingstone, 2008.
- [22] J.D. Willson, S. Binder-Macleod and I.S. Davis, "Lower extremity jumping mechanics of female athletes with and without patellofemoral pain before and after extension," *American Journal of Sports Medicine* 36, 2008.